DEVELOPMENT OF A THEORY OF THE SPECTRAL REFLECTANCE OF MINERALS PART II

by

J. R. ARONSON, A. G. EMSLIE, L. H. ROACH,
P. F. STRONG, AND P. C. VON THŮNA

APRIL 1, 1971

NAS 9-10875

ADL C-72594

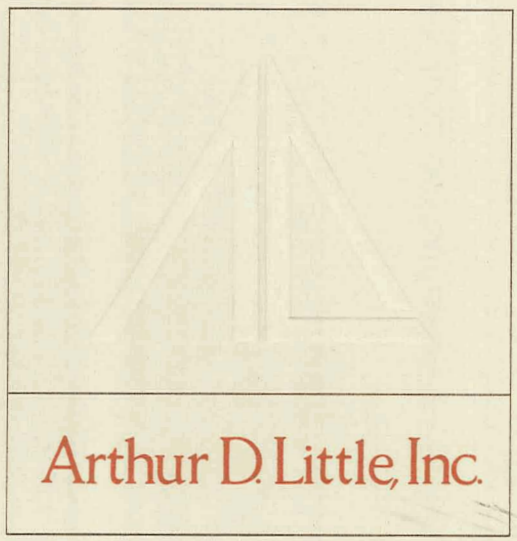

Arthur D. Little, Inc.

CR-115059

DEVELOPMENT OF A THEORY OF THE SPECTRAL REFLECTANCE OF MINERALS PART II

By

J. R. Aronson, A. G. Emslie, L. H. Roach,
P. F. Strong, and P. C. von Thüna

Prepared for

National Aeronautics and Space Administration
Manned Spacecraft Center
Houston, Texas 77058

Interim Technical Summary Report

Contract NAS 9-10875
ADL C-72594

April 1, 1971

Arthur D. Little, Inc.

Abstract

Considerable progress has been made in refining the previously reported theory of the diffuse reflectance of particulate media.

A more accurate calculation of the absorption loss in the particles has been made and a factor allowing for interparticle contacts has been included. With these changes, reasonably good fits are obtained to experimental data for quartz, garnet, glass, corundum powders, and mixtures of these for particle sizes down to $d \sim \lambda$. The observed particle dependence is now qualitatively given by the theory. For fine particles a modified Lorentz-Lorenz theory that allows for the skin depth of the radiation has been tried. It appears to indicate that clumping of the particles must be taken into account. The principal remaining unresolved problem is the inadequate behavior of the theory in regions of anomalous dispersion where $n << 1$. This is particularly evident in the case of corundum between 650 cm^{-1} and 850 cm^{-1}. A number of possible explanations of the discrepancy are considered.

TABLE OF CONTENTS

TABLE OF CONTENTS (continued)

LIST OF TABLES

LIST OF FIGURES

LIST OF FIGURES (continued)

I. INTRODUCTION

At the beginning of this contract, several years of research had led to the development of a two part theory of reflectance of particulate solids. The theory was based on fundamental principles of optics and guided by a small number of low resolution experiments on the infrared reflectance and emittance spectra of powders. These powders consisted of relatively coarse quartz samples (separated by dry sieving and obtained from Dr. Thomas Rooney of the Air Force Cambridge Research Laboratories) and somewhat finer corundum samples obtained from the Microabrasives Corporation of Westfield, Massachusetts. The reasons for the choice of these powders have been previously explained,[1,2] but there were some unsatisfactory factors involved in their use. The quartz samples were contaminated with an admixture of fines remaining from the dry sieving separations and the finest sample (< 53μ) was insufficiently separated so as to adequately define its effective particle size. One further quartz sample having a bimodal size distribution in the 10μ-20μ region was also studied and its characteristics were somewhat different from those of the coarser (> 53μ) quartz powders. The corundum samples suffered from an approximate 5:1 aspect ratio of the particles so that once again the particle sizes were somewhat uncertain. However, they were all in the particle-size range less than 30μ.

The two parts of our theory consisted of a coarse-particle theory based on geometrical optics and a fine-particle theory based on Rayleigh scattering and the Lorentz-Lorenz theory of dielectrics. Computer calculations indicated that the spectra of the quartz powders (except the 10μ-20μ sample) were reasonably well fitted by the coarse-particle theory in general shape but that only certain bands had the type of particle size dependence predicted by the theory (Figures 1a and 1b). In fact, for particles in the size range studied experimentally the coarse-particle theory always produced greater reflectance with diminished particle size. In addition, the rate of change of reflectance was much less in practice than in theory. The fine-particle theory

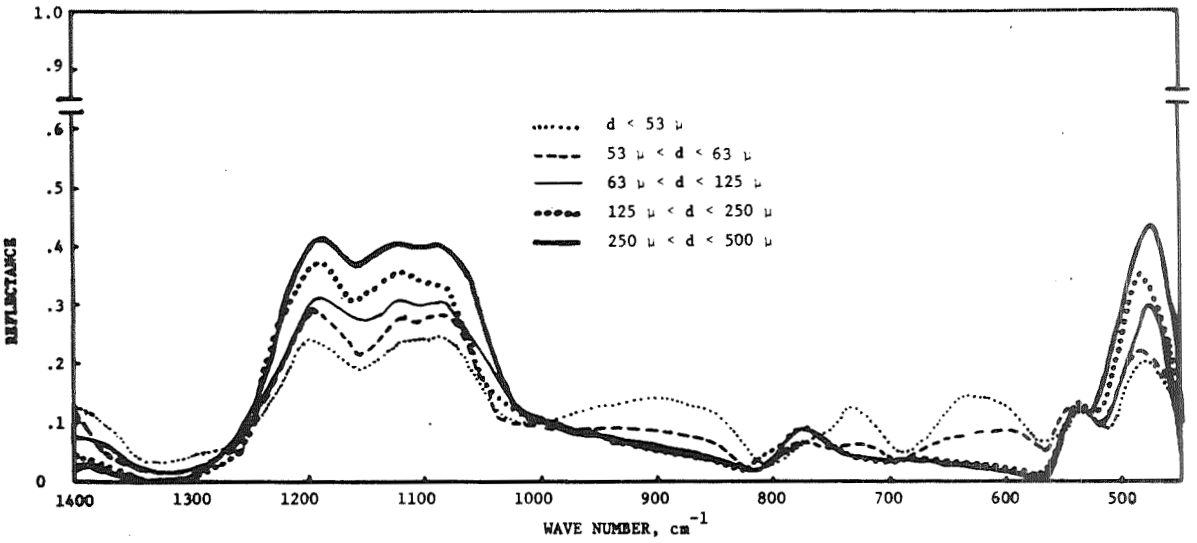

FIGURE 1a. EXPERIMENTAL REFLECTANCE OF QUARTZ POWDERS (LOW RESOLUTION).

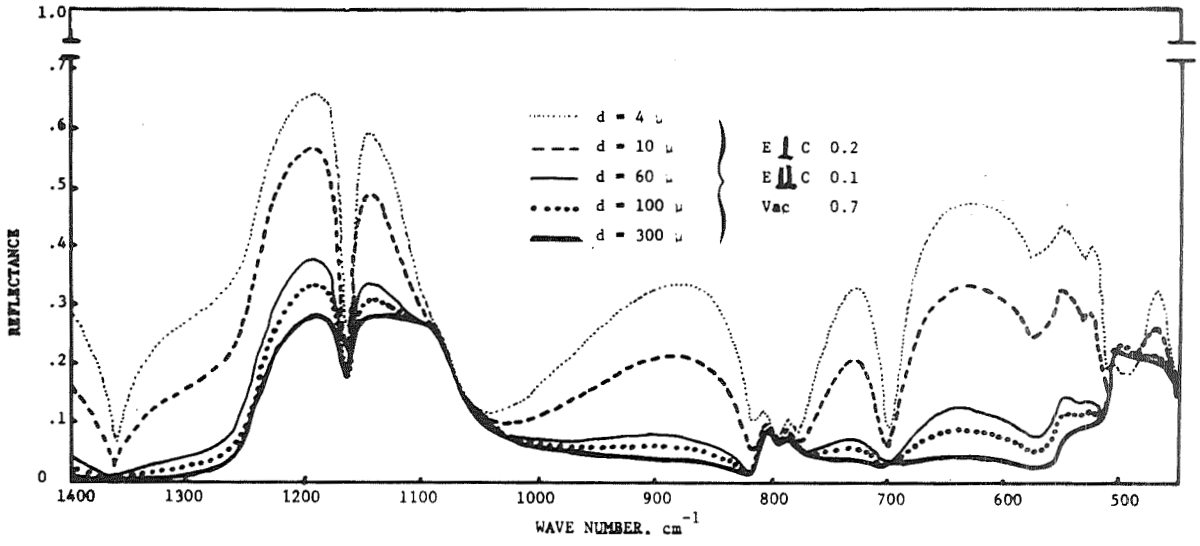

FIGURE 1b. THEORETICAL REFLECTANCE OF QUARTZ POWDERS (1970).

appeared necessary in the case of the corundum powder, but a fairing-in of the coarse-particle theory in certain spectral regions was necessary to adequately represent the overall shape of the spectrum. This was not arbitrarily carried out, but was guided by a criterion based on the fine-particle theory calculations, which produced a scattering cross-section orders of magnitude larger than physically reasonable. Thus we assumed that in such spectral regions the theory was carried beyond its range of applicability. Using the fine-particle theory together with the coarse-particle theory in certain spectral regions, we were able to produce the fit shown in Figure 2a. The region near 800 cm^{-1} could not be fitted by either theory and was our principal concern (Figure 2b).

Both subtheories require knowledge of the spectral behavior of the refractive index and absorption coefficient for each of the minerals involved together with their particle sizes and volume fractions. These fundamental parameters were used to calculate internal and external "surface" reflectance terms according to the Fresnel equations and a volume term calculated from the Kubelka-Munk two-beam equations of radiative transfer. The calculation of the microscopic absorption and back-scattering coefficients from the fundamental parameters is the most vital part of the entire theory. It had been based on a random interface model.

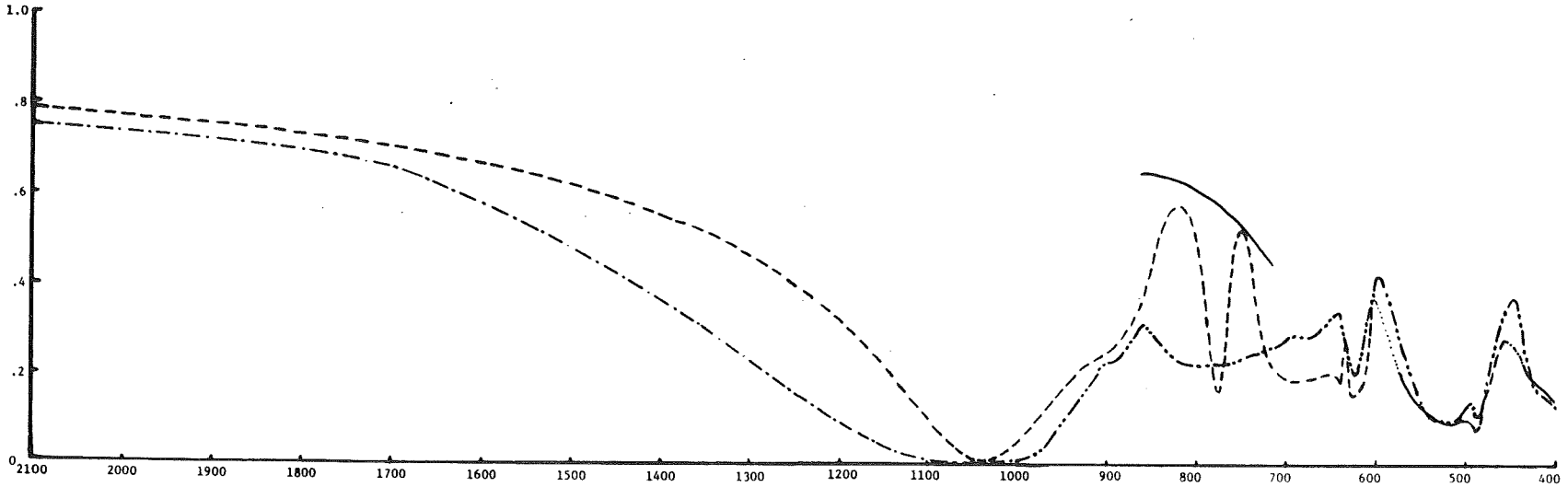

FIGURE 2a. THEORETICAL AND EXPERIMENTAL REFLECTANCE OF CORUNDUM POWDER (1970).

LEGEND:

FIGURE 2a.

EXPERIMENTAL 30 WCA

REFLECTANCE (NBS)

1-EMITTANCE (ADL)

THEORETICAL

COARSE-PARTICLE THEORY

E⊥C 0.25 d = 6 μ
E∥C 0.05 d = 30 μ
VAC 0.70

FINE-PARTICLE THEORY

E⊥C 0.2 d_e = 6 μ
E∥C 0.1
VAC 0.7

FIGURE 2b.

R_e (COARSE)

R_e (FINE$_1$)

R_e (FINE$_2$)

R_v (FINE$_1$)

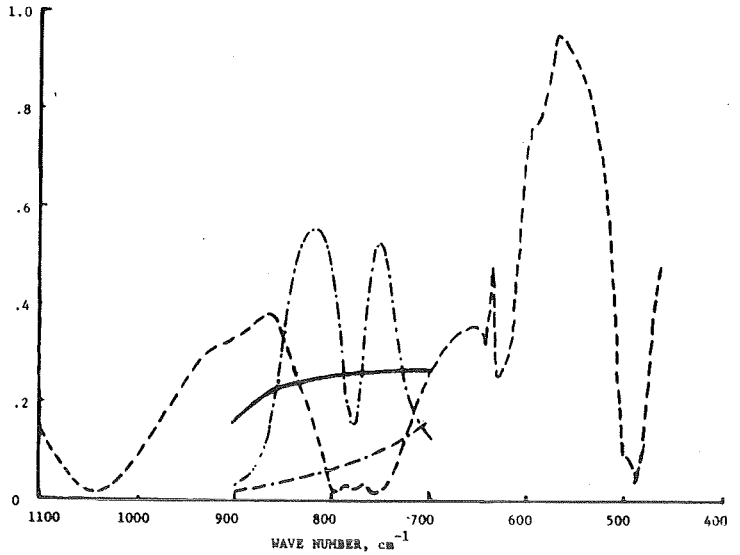

FIGURE 2b. COMPONENTS OF THEORETICAL REFLECTANCE OF CORUNDUM POWDER (1970).

II. THEORETICAL DEVELOPMENTS

A. IMPROVEMENTS IN THE COARSE-PARTICLE THEORY

At the start of the present contract period our theory for a powder consisting of coarse particles took the form of a statistical model in which the particles are replaced by a series of randomly oriented interfaces separating regions of refractive index $m = n-ik$ from void regions of index 1. In the model, the intensity of the radiation at a given depth below the surface of the powder is taken as a local average of the intensities in the two regions, the intensity in the regions of index m being n^2 times as large as that in the void regions.

A weakness of this model is that in a reststrahlen band where the absorption index k is large the particles become opaque and the n^2 intensity factor, which is valid for transparent particles, becomes a rather poor approximation. To avoid this difficulty we have changed the definition of the radiation intensity at any point in the powder to be the local intensity in the voids.

This change in definition of the intensity results in a simplification in the boundary condition at the surface of the powder. Since the external void space merges continuously into the void spaces in the powder, the incident radiation also merges continuously into the forwards-directed part of the diffuse radiation in the void spaces in the powder. Therefore, there is no longer any need to include external and internal surface reflectances as in the previous model.

In support of the new point of view it is to be noted that the Kubelka-Munk theory of diffuse light propagation in pigments gives very good agreement with experiment without taking surface reflection into account. On the other hand, we have found (in a study for the Boxboard Research and Development Association) that our previous theory also works well for pigments such as clay and titanium dioxide, which are highly

transparent in the visible part of the spectrum. It turns out in this case that the older theory gives a much higher value of the scattering coefficient S, but that the increase in scattering efficiency is almost exactly compensated by the large internal surface reflection that results from the inclusion of the radiation within the pigment particles in the definition of the light intensity in the powder. However, in the case of strongly absorbing particles in the infrared region of the spectrum, balancing of the two effects is not to be expected.

In the amended theory, we calculate the scattering as before by means of the random interface model. Since, however, we no longer take account of the radiation intensity inside the particles, we must now consider the effect of a pair of interfaces belonging to the same particle. The diffuse reflectance R of such a pair of interfaces can be calculated approximately as though the particle were a parallel-sided plate of effective thickness d. The result is

$$\bar{R} = \bar{R}_o + \frac{\bar{R}_o(1 - \bar{R}_o)^2 e^{-2\alpha d}}{1 - \bar{R}_o^2 e^{-2\alpha d}} \qquad (1)$$

where $\bar{R}_o$ is the diffuse external reflectance of one interface and $\alpha = 4\pi k/\lambda$ is the absorption coefficient of the particle material. This formula is based on incoherent addition of the multiple reflections from the two interfaces. The distance d is the effective separation of the pair of interfaces for diffuse radiation, which is of the order of twice the mean separation.

The contribution of reflection to the backscattering coefficient S is

$$S_{\text{reflection}} = \frac{1}{2} \sum_j N_j \bar{R}_j \qquad (2)$$

where $\bar{R}_j$ is the value of $\bar{R}$ for mineral j and N_j is the average number of interfaces of mineral j per unit length of any line in the powder. The factor of 1/2 includes a factor of 2 to allow for the greater path taken on the average by diffuse radiation relative to that for a parallel beam, a factor of 1/2 to allow for the portion of the reflection that is backscattered, and a factor of 1/2 to allow for the fact that (2) includes the combined reflections of two interfaces.

The average transmittance $\bar{T}$ through a pair of interfaces is given by

$$\bar{T} = \frac{(1 - \bar{R}_o)^2 e^{-\alpha d}}{1 - \bar{R}_o^{\,2} e^{-2\alpha d}} \tag{3}$$

The contribution of this refracted radiation to S is given by

$$S_{\text{refraction}} = \frac{\sqrt{2}}{2} \Sigma N_j \bar{T}_j \cdot \left(\frac{2}{\pi} \frac{\sin\phi_{m,j} - \phi_{m,j} \cos\phi_{m,j}}{1 - \cos\phi_{m,j}} \right) \tag{4}$$

where

$$\begin{aligned} \cos\phi_{m,j} &= \frac{1}{n_j} && (n_j > 1) \\ &= n_j && (n_j < 1) \end{aligned} \tag{5}$$

The expression in parenthesis, which is derived in our previous reports,[1,2] gives the fraction of the refracted radiation that is backscattered. The factor $\sqrt{2}$ allows for the random addition of the deflections due to refraction at the two interfaces. The factor 1/2 allows, as before, for the fact that (4) is the contribution of two interfaces.

The total backscattering coefficient S is the sum of (2) and (4):

$$S = S_{reflection} + S_{refraction} \tag{6}$$

At the center of a strong absorption band where α_j is large, the contribution of $S_{refraction}$ becomes negligible owing to the factor T_j. At the same time $S_{reflection}$ reduces to the contribution of front surface reflections $\overline{R}_{o,j}$ by each pair of interfaces of type j, according to (1).

The revised coarse-particle theory also includes an improved way to calculate the absorption coefficient K of the powder. From (1) and (3) we can immediately obtain the absorbance $\overline{A}_j$ of a given pair of interfaces:

$$\overline{A}_j = 1 - \overline{R}_j - \overline{T}_j \tag{7}$$

The absorption coefficient K is the average absorbance per unit distance of travel of a diffuse beam of radiation. Therefore

$$K = \Sigma N_j A_j \tag{8}$$

In this formula a slant path factor of 2 is canceled by a pair factor of 1/2.

The factor N_j in expressions (2), (4), and (8) is given by the formula

$$N_j = \frac{f_j s_j}{2v_j} \tag{9}$$

where f_j is the volume fraction of mineral j, s_j is the mean surface area

of type-j particles and v_j is the particle volume. For rectangular particles of dimensions a_j, b_j, c_j Eq (9) becomes

$$N_j = f_j\left(\frac{1}{a_j} + \frac{1}{b_j} + \frac{1}{c_j}\right) \tag{10}$$

For spheres of diameter d_j the relation is

$$N_j = \frac{3f_j}{d_j} \tag{11}$$

The theory presented so far should give a good approximation for S and K for particles that are reasonably large and reasonably well separated compared with the wavelength of the radiation. However, in a powder of coarse particles the gaps between the particles are not large compared with the wavelength, in the immediate neighborhood of the points of contact between the particles. In such areas there is an almost perfect optical bond between adjacent particles wherever the inter-particle gap is of the order of a tenth of a wavelength. This effect causes an important loss of scattering efficiency for both reflective and refractive scattering. To allow for this loss we must multiply S by a suitable "contact factor."

We will assume that the contact factor is equal to the fraction of the surface area of a particle remaining after subtracting the areas around the contact points that are almost completely bonded optically. The area lost at each contact point is related to the size of the central dark fringe of the Newton's ring interference pattern at the contact point. The reflectance of the gap is zero at the point of contact and reaches the first maximum where the gap thickness is $\lambda_o/4$, where λ_o is the free space wavelength of the radiation. We therefore assume as a rough approximation that complete optical bonding occurs at all points

where the gap is less than $\lambda_o/10$ and that the two interfaces act independently of each other everywhere else. For the case of spheres of diameter d the gap g at a distance r from a contact point is given approximately by

$$g = \frac{2r^2}{d} \tag{12}$$

Therefore, for $g = \lambda_o/10$ we find for the optically bonded area at each contact point:

$$a = \pi r^2 = \frac{\pi d \lambda_o}{20} \tag{13}$$

The total optically bonded area per sphere depends on the number of contact points N_c, which in turn depends on the volume fraction f occupied by the particles. We can derive a relation between N_c and f by considering the various regular arrangements of spheres as shown in Figure 3. From these numbers we obtain the formula

$$N_c = 12\ f \tag{14}$$

which is approximately correct for $f < 0.7$. We will assume that Eq (14) is valid also for randomly distributed particles.

The total area of each sphere lost by optical bonding is $\pi r^2 N_c$. The contact factor G is the fraction of the surface area πd^2 that is left for reflection and refraction:

$$G = 1 - \frac{a}{\pi d^2} N_c = 1 - \frac{3}{5} \frac{f \lambda_o}{d} \tag{15}$$

The scattering coefficient S, which is the sum of the reflection and refraction contributions given by expressions (2) and (4), must

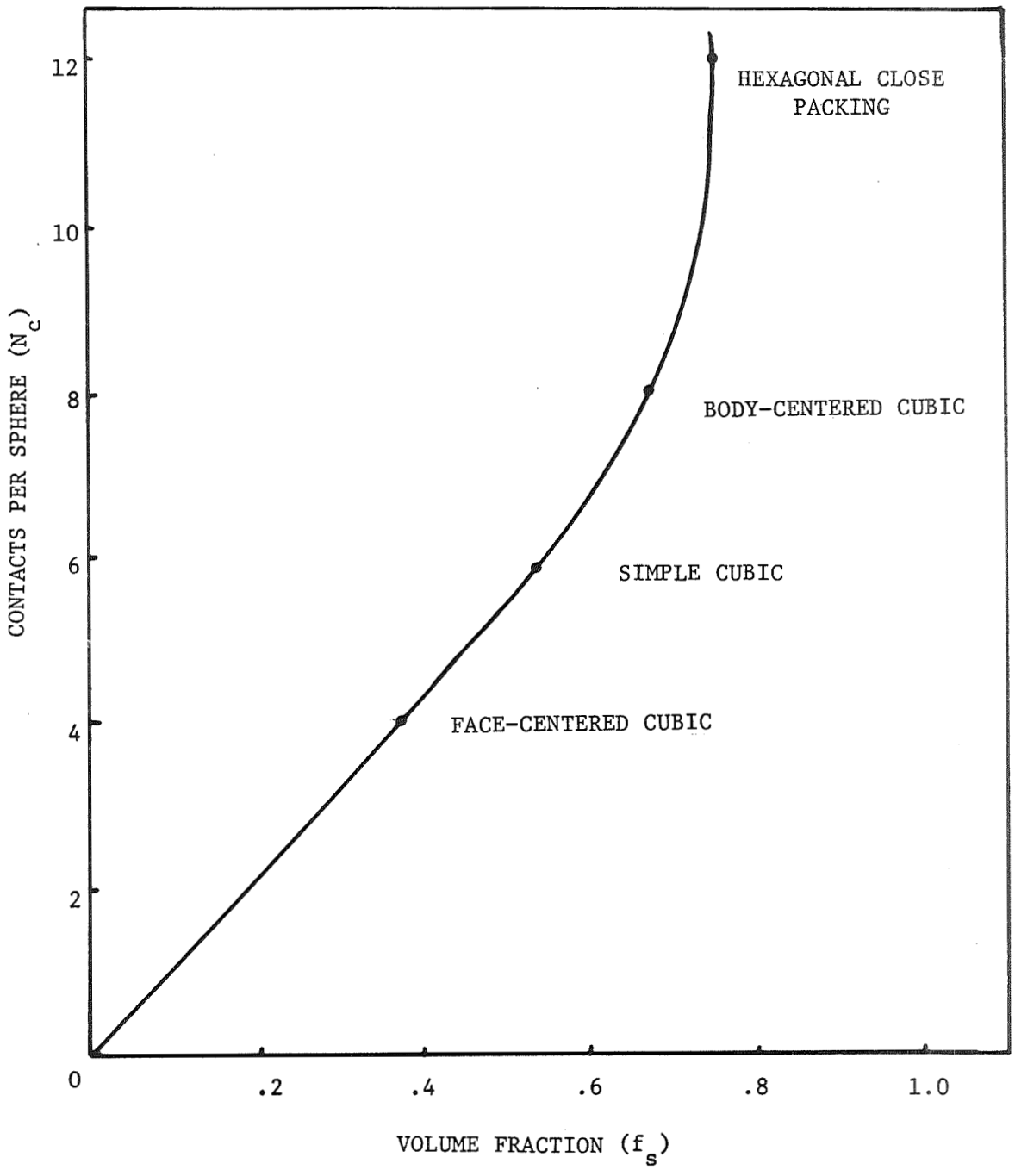

FIGURE 3. NUMBER OF CONTACTS PER SPHERE

be multiplied by the contact factor G. The corrected value of S, from (10) and (11) is therefore proportional to G/d. This explains why with decreasing particle size the scattering efficiency at first increases as 1/d but ultimately falls off rapidly to low values. By maximizing G/d with respect to d one can show that the maximum value of S occurs when the contact factor is 1/2.

A weakness of Eq (15) is that it predicts that the contact factor G becomes zero for a certain critical value of d. This results, of course, from our "all or nothing" treatment of optical bonding. The formula should be refined to include the effect of continuously variable optical bonding. Eq (15) does, however, correctly depict the main features of optical bonding.

The diffuse reflectance R_v of the powder is related to the back-scattering and absorption coefficients S and K by the Kubelka-Munk formula

$$R_v = 1 + \frac{K}{S} - \sqrt{\frac{K^2}{S^2} + 2\frac{K}{S}} \tag{16}$$

If the incident radiation is collimated, the reflectance is modified slightly to the form

$$R = \frac{2 R_v}{3 - R_v} \tag{17}$$

Eq (17) is the correct form to use if one wishes to calculate the normal emittance ε_n of the powder by means of Kirchhoff's formula

$$\varepsilon_N = 1 - R \tag{18}$$

B. NEW FINE-PARTICLE THEORY

We will show in a later section that the present coarse-particle theory based on geometrical optics, with a correction for wave interference in the gaps between particles, gives good agreement with experiment for quartz powders even when the particle size is not too much greater than the wavelength. For still smaller particles one expects that wave interference within the particles, as well as in the gaps, will become important and that optical bonding between particles (contact factor) will be enhanced. Under these conditions the powder should behave optically more like a continuous medium than a scattering medium, provided that the particles are distributed quite uniformly in space, i.e., not clumped. We therefore need a theory, based completely on wave optics, for calculating the average index of refraction of such a fine-particle medium.

We have previously attempted to extend the Lorentz-Lorenz theory of the dielectric constant from the case of molecular-sized particles to particles of macroscopic size. This attempt was only partially successful because, we believe, the Lorentz-Lorenz theory represents the radiative coupling between the particles in terms of dipole interaction only. In the case of particles with strong reststrahlen bands the radiation may penetrate only a fraction of the diameter of the particle. Under these conditions the dipole approximation is very poor. We have therefore taken a new approach to the problem which allows for the rapid attenuation of the waves in the particles.

As in the Lorentz-Lorenz theory we consider a spherical particle of radius a and complex index m_p located at the center of a spherical cavity of radius b in a continuous medium of complex index m. The radius b is chosen so that the empty volume around the particle is equal to the particle's share of the void space in the powder, i.e.,

$$b = \frac{a}{f^{1/3}} \tag{19}$$

The continuous medium represents the average effect on the central particle of all other particles and the problem is to determine the average index m of this medium of smeared-out particles. To do this we apply a self-consistency criterion that for an ingoing spherical wave in the continuous medium the reflected wave is unchanged if the central particle and its surrounding layer of void space are replaced by medium of index m.

We consider only scalar waves on the ground that such waves usually give a reasonable approximation to the average behavior of the two states of polarization of electromagnetic waves. The waves in the three regions, which are solutions of the Helmholtz equation

$$\nabla^2\phi + K^2\phi = 0 \qquad (20)^*$$

are

$$\phi_{particle} = A\, j_o\,(K_p r) \qquad (21)$$

$$\phi_{gap} = B\, j_o\,(K_o r) + C\, y_o\,(K_o r) \qquad (22)$$

$$\phi_{medium} = D\, j_o\,(Kr) \qquad (23)$$

where j_o, y_o are spherical Bessel functions of order zero, $K_p = 2\pi\nu m_p$, $K_o = 2\pi\nu$, $K = 2\pi\nu m$, and ν is the frequency in wavenumbers. The Bessel functions have the form

$$j_o(z) = \frac{\sin z}{z} \qquad (24)$$

$$y_o(z) = \frac{\cos z}{z} \qquad (25)$$

Since $\phi_{particle}$ must be finite at the origin, Eq (21) contains

---

*The wave vector K in this equation is not to be confused with the Kubelka-Munk absorption coefficient K.

only j_o. Likewise (23) contains only j_o since according to our criterion this equation must remain the same (and be everywhere finite) when the cavity is filled with the same medium.

The waves given by (21), (22), and (23) have to satisfy the boundary conditions that ϕ and $\partial\phi/\partial r$ are continuous at r = a and r = b. This gives four linear homogeneous equations in the amplitudes A, B, C, and D. For consistency the determinant of the coefficients of these four equations must be zero, which gives the relation

$$\begin{vmatrix} j_o(K_o a) & y_o(K_o a) & j_o(m_p K_o a) & 0 \\ j_o'(K_o a) & y_o'(K_o a) & m_p j_o'(m_p K_o a) & 0 \\ j_o(K_o b) & y_o(K_o b) & 0 & j_o(mK_o b) \\ j_o'(K_o b) & y_o'(K_o b) & 0 & m j_o'(mK_o b) \end{vmatrix} = 0$$

where the primes indicate first derivatives.

On expanding the above determinant and collecting the terms containing $mK_o b$ we get an equation of the form

$$\frac{z}{\tan z} = W \qquad (26)$$

where $z = 2\pi\nu bm$ and W is a function of the known quantities m_p, ν, a, and b.

Since the solution to Eq (26) is multivalued we have to start the computer calculation with a situation for which the solution is known. Such a case is where f = 1 (i.e., b = a), for which m is clearly equal to m_p. We then change f by small steps and solve Eq (26) by

Newton's method using the previously found value of m as the starting value in Newton's procedure. Of course, W has to be re-evaluated at each step since it is a function of f. This method of solution proves to be workable provided that b and a are reasonably small compared with the wavelength. In other words, the computation presents no difficulties under conditions where the concept of an average index of refraction of the powder is meaningful.

If we attempt to extend the method to particle sizes and spacings of the order of the wavelength or larger, the calculated values of m as a function of ν show discontinuities which indicate that the solution jumps from one branch to another of the multiple valued function z(W). These jumps are associated with the breakdown of Newton's method of obtaining the roots of Eq (26) when the trajectory in the z-plane corresponding to stepping in f comes close to a branch point of Eq (26), i.e., to a value of z for which $dW/dz = 0$. It appears that the root jumping behavior indicates that the particles are so large or so widely spaced that the concept of a unique average index of refraction does not apply to the system.

The values of z, and the corresponding values of W, for the first three branch points of Eq (26) are as follows:

z	W
3.75 - 1.38 i	2.90 + 3.72 i
6.95 - 1.68 i	3.18 + 6.93 i
10.12 - 1.86 i	3.36 + 10.11 i

A rough criterion for the applicability of the fine-particle theory is therefore that the constants m_p, ν, a, and b must be such that

$$|W| \leq |2.90 + 3.72\ i| = 4.71 \qquad (27)$$

We have checked this criterion for the case of 2μ particles of corundum for f = 0.3. The criterion is satisfied over almost the whole spectrum and the computed value of m(ν) shows no evidence of branch jumping. Figures 4 and 5 show plots of n(ν) and k(ν) for a powder of 2μ corundum particles with an overall volume fraction of 0.3 ($E \perp C = 0.2$, $E \parallel C = 0.1$). Also shown are the values of n_p and k_p for both orientations of corundum and the predictions of the Lorentz-Lorenz theory.

It is seen that the average indices calculated from the spherical wave model have the general shape of the particle indices but are reduced by the effect of the voids. This appears to us to be an improvement over the Lorentz-Lorenz fine-particle theory.

The Fresnel surface reflectance of the powder computed from the spherical wave model values of n and k of Figures 4 and 5 is shown in Figure 6 in comparison with the measured reflectance for 10μ corundum particles. One sees that the theoretical spectrum is much too high and any changes with particle size between 2μ and 10μ will be unable to remedy the problem.

The most likely reason for this disparity is that the fine particles are not uniformly dispersed as assumed in the theory. Microscopic examination of the powder samples indeed shows that the distribution of the particles is far from uniform for the finer particles. Under these conditions we should use a clump model and conclude, as in the case of the coarse-particle theory, that the contribution of the Fresnel surface reflection should be omitted. For fine as well as for coarse particles, therefore, only volume reflection is to be included. The volume reflection for fine particles will in general consist of two parts--Fresnel reflection from the surface of clumps and Rayleigh scattering from the individual particles within the clumps. In this report we will deal only with the Rayleigh contribution.

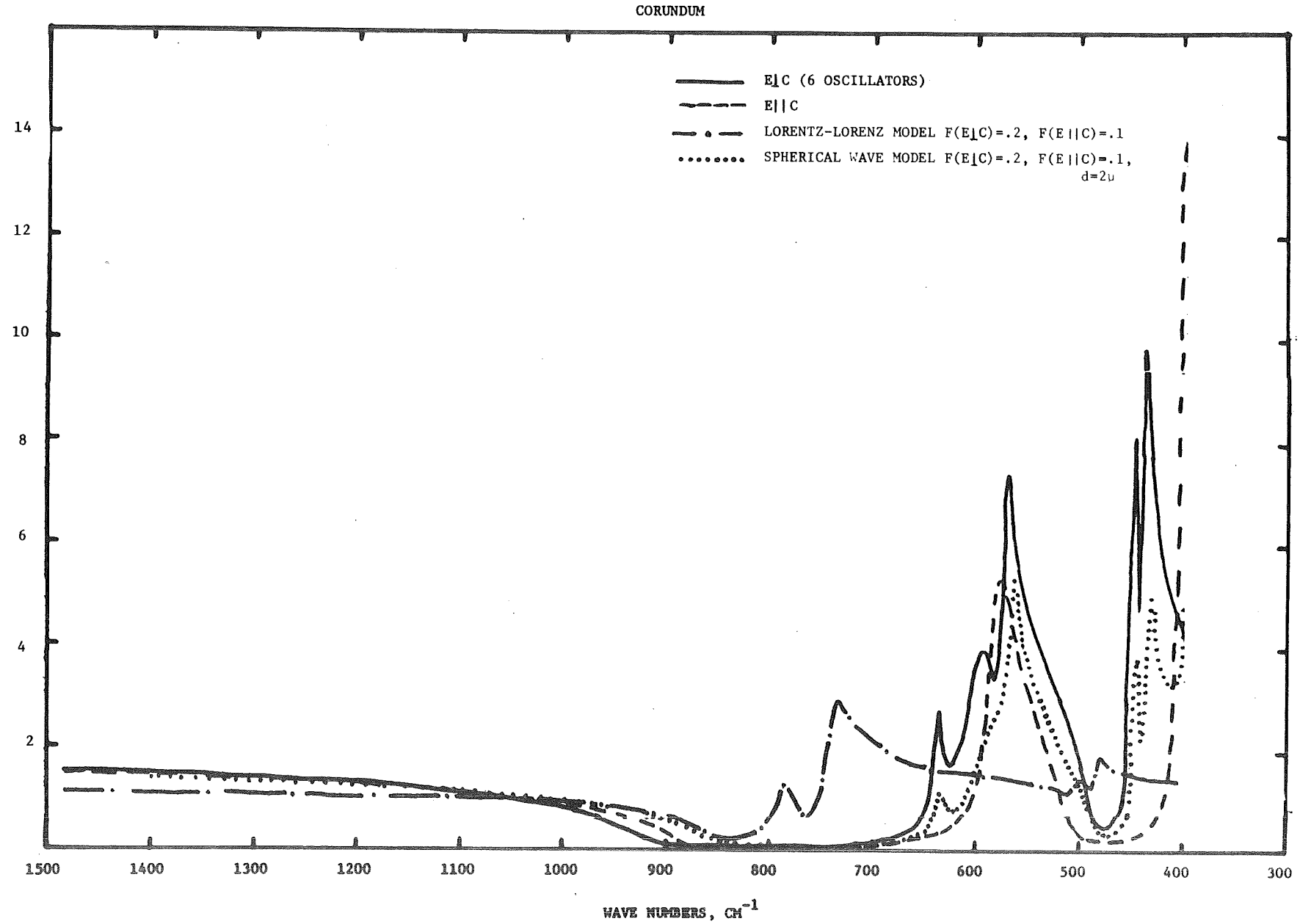

FIGURE 4. REFRACTIVE INDEX OF CORUNDUM.

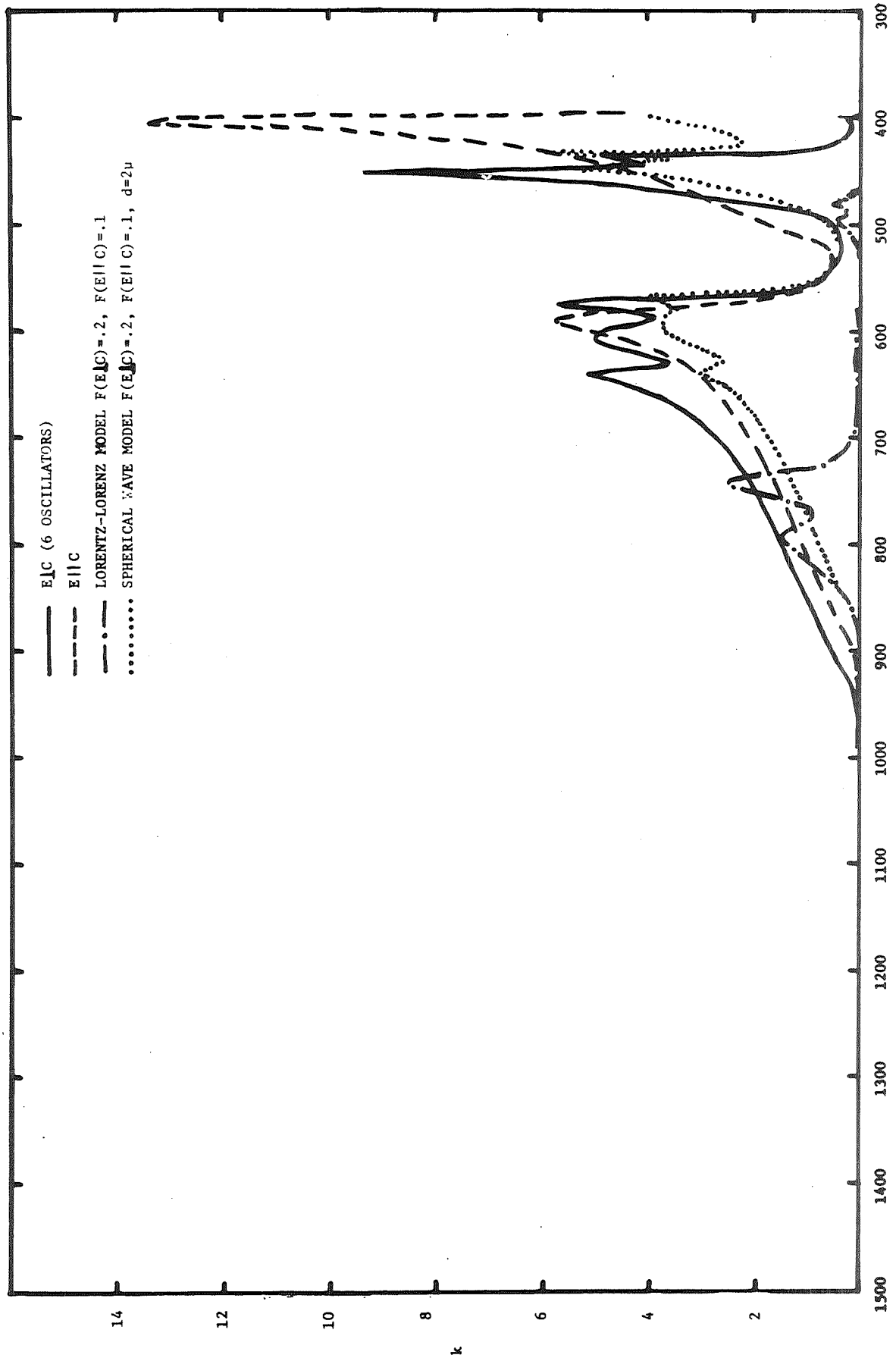

FIGURE 5. ABSORPTION INDEX OF CORUNDUM.

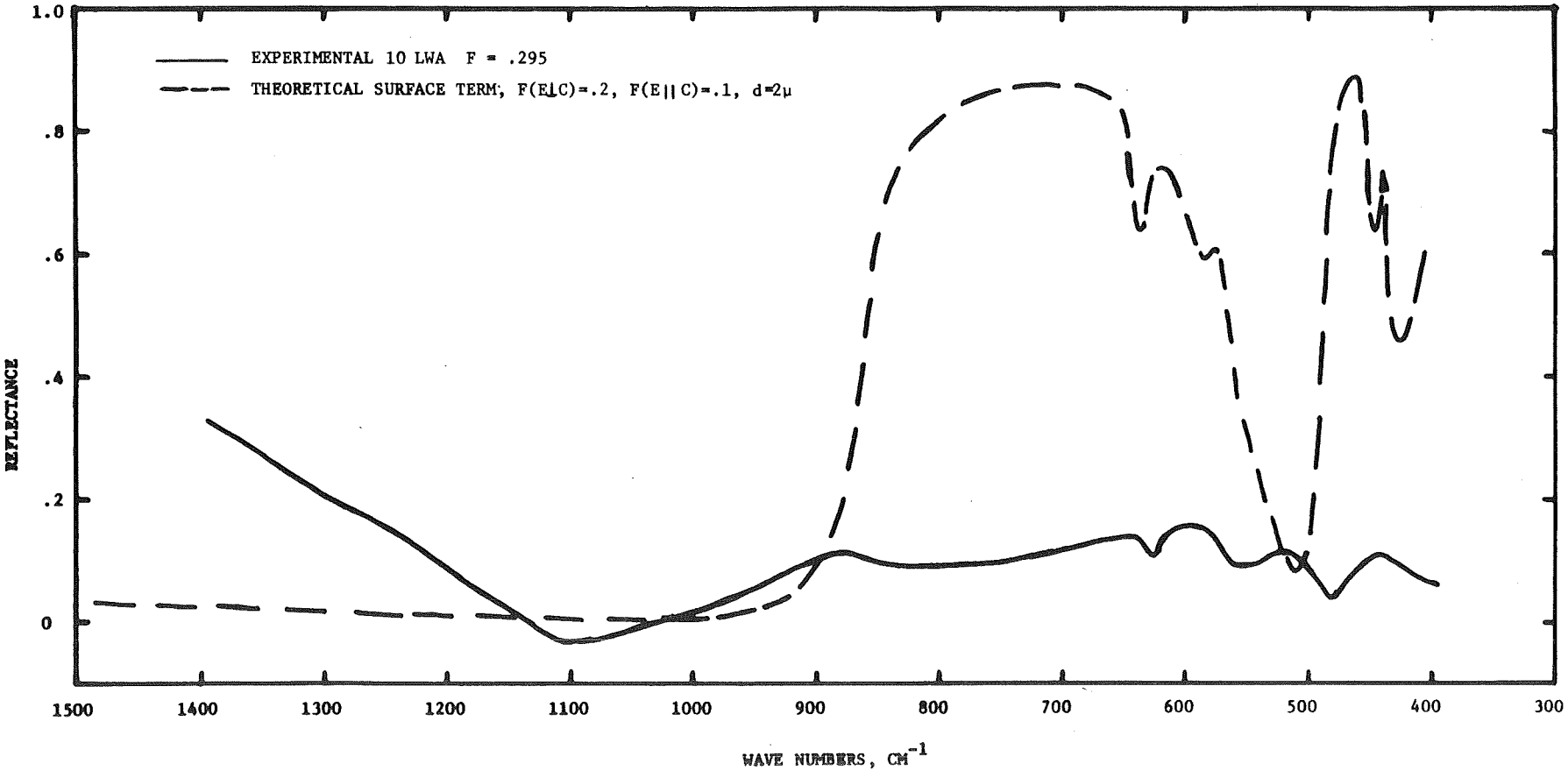

FIGURE 6. FAILURE OF A THEORETICAL SURFACE TERM TO PRODUCE AGREEMENT WITH EXPERIMENT.

To calculate the Rayleigh scattering we consider each particle in a clump to be surrounded by a medium that has the average index of refraction n given by the new theory (spherical wave model) described above. The contrast between this index and the index n_p of the particle gives rise to scattering proportional to $(n_p^2 - n^2)^2$, while the voids, of index 1, give a contribution proportional to $(1 - n^2)^2$. These contributions are weighted with respect to the two volume fractions. The details of the Rayleigh scattering theory are given in our earlier reports.[1,2]

III. EXPERIMENTAL MODIFICATIONS

The apparatus for our emittance measurements using Fourier spectroscopy was described in our previous reports.[1,2] At the inception of this work we proceeded to carry out a number of powder emittance measurements. We immediately ran into various experimental difficulties that in retrospect appear to have resulted from a variety of intermittent peripheral problems. These were such as to give dubious, somewhat variable results. We concluded that an overhaul of the system was in order, and this involved a variety of changes.

The interferometer itself was optically realigned and mounted on a spring-suspended platform in such a way as to eliminate mechanical vibrations. Horizontal accelerations in particular have been found to impair resolution of the instrument and the platform was especially designed to deal with this problem (see Figure 7). The usual electrical frequencies in our measurements have ranged from about 2 to 10 Hz. In order to have somewhat more flexibility in this regard, the passband of the signal amplifiers was extended. We hoped to take advantage of the reduction of mechanical vibrations by our new spring-mounted platform (resonance frequency near 1 Hz), and the expected decrease in interferometer drive noise at higher frequencies. Barnes Engineering Company reported that the signal-to-noise ratio of the triglycine sulfate pyroelectric detector falls only slowly between 10 and 100 Hz. In practice, higher frequency operation has proved to be of no advantage. The pulses produced by both the white light and laser channels proved to be somewhat erratic and the causes for this were tracked down and remedied. Further improvement in this area will result when a new beamsplitter (made entirely out of KRS5) is installed. As we were originally in the position of having to process our data all the way through our IBM System 360 before we knew if there were troubles with each experiment, a number of diagnostic realtime computer programs were written that have made check-out and troubleshooting much faster and simpler.

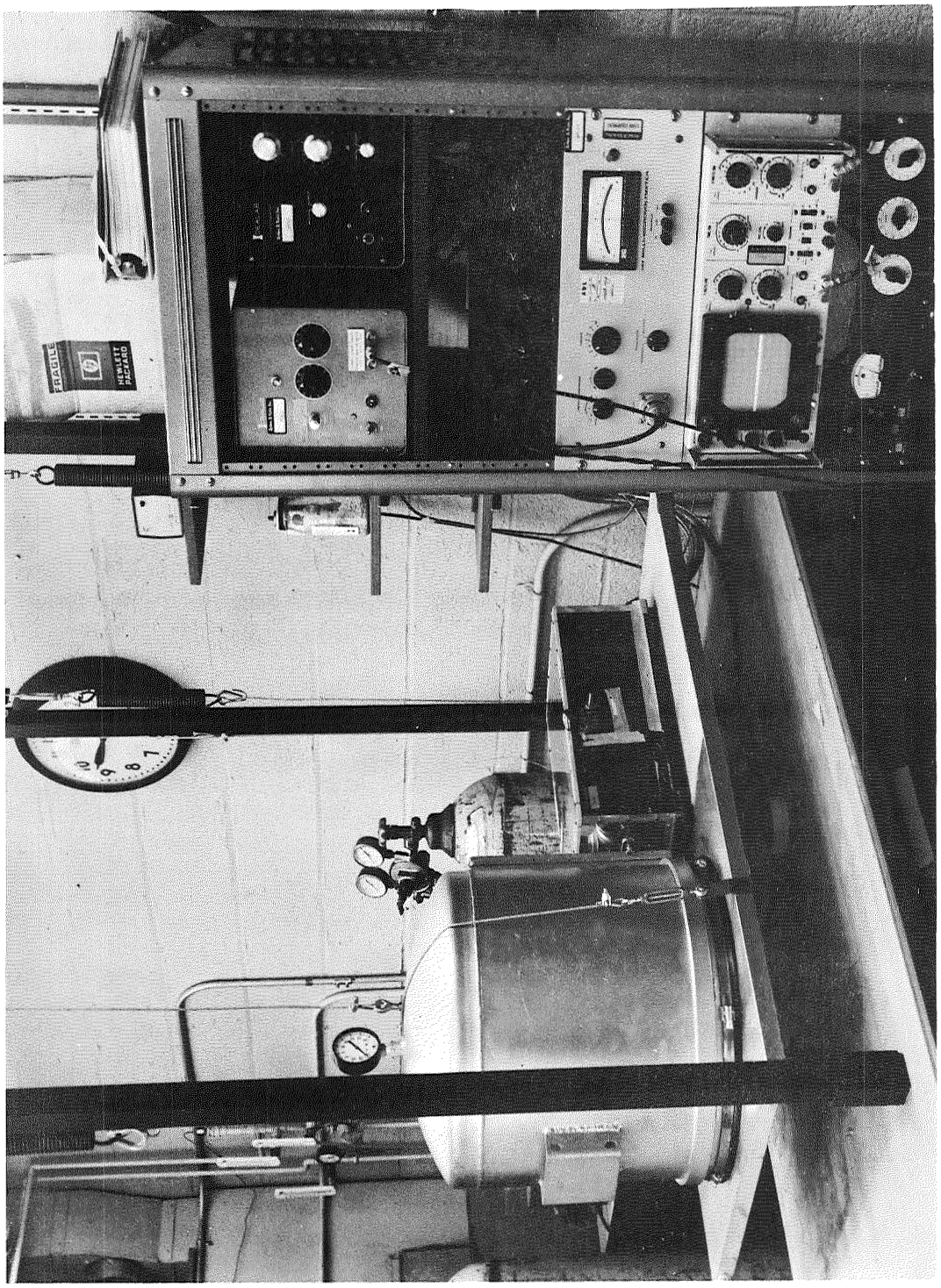

FIGURE 7. INTERFEROMETER SYSTEM.

Reruns of data previously obtained indicated that the background spectra have gradually changed with time and that our method of carrying out double-beam experiments with sample and "blackbody" runs[1,2] did not entirely compensate for this effect. This was proven by making a number of "blackbody" runs at different temperatures and finding that if one was treated as a sample, some deviation from a straight line at unit emissivity was produced by our method. This is understandable if any elements in the optical train have appreciable absorption and therefore emission spectra. Our program would compensate for transmission or reflection losses but not for self emission terms. These can be important and result in some deviations from proper values of sample emittance as the measurements are all made at temperatures near ambient. To eliminate this problem a new calibration scheme was worked out based on the measurement of two different "blackbody" radiances immediately before or after the sample measurements. This involves little additional effort as the bulk of the time required for measurements is spent waiting for thermal equilibrium to be established in our sample chamber. The details of the new calibration technique are given in Appendix A. As a result of our analysis we are currently operating the shield for our measurements at room temperature as it is entirely unnecessary to cool this shield to cryogenic temperatures as long as its temperature and emittance are sufficiently well known.

This result together with the desire to be able to operate under vacuum and our experience with our previous sample chamber led us to construct an improved version.

The new sample chamber (see Figure 8) is designed to be vacuum tight and is equipped with pumps and gauges thus allowing us to work at any pressure in a clean and well defined artificial atmosphere or in a vacuum. By imaging the aperture of the interferometer cube on the sample with a demagnification factor of 1.5, the total required sample volume has been reduced to approximately 2.5 cc and the optically effective surface area to approximately 2.3 cm^2. Our present sample volume is

FIGURE 8. EMITTANCE OPTICS.

well oversized at 11.58 cc with a surface area of 10.5 cm^2. The figure shows the sample turntable, the black cavity, and the top of the vacuum chamber. A simple pressure gauge enables us to backfill conveniently with dry nitrogen. A Pirani vacuum gauge is used during high vacuum work.

The principal problem in making sample emittance measurements is that of temperature measurement. We measure the cavity, interferometer, "blackbody" and sample tray temperatures by means of precalibrated precision thermistors. The departure from cryogenic techniques has made the net heat flow to the cavity negligible and this has greatly eased our concerns about the isothermal character of our black cavity.

The principal remaining problem in temperature measurement is to find the appropriate "surface" temperature for the powder. To this end we have stretched copper-constantan differential thermocouples of 2-mil diameter horizontally across the sample tray at different heights. The first pair measures the difference between the sample tray temperature and a station 0.719 cm above the tray. The second pair measures the difference between that station and a second station 0.254 cm higher and 0.127 cm below the nominal surface (see Figure 9). The "surface" temperatures thus estimated produce emittance curves that generally appear to be within 0.5°C of the temperature inferred from the Christiansen frequency technique previously used.[3] There were, however, a few cases of significantly larger errors. One source of error in this technique occurs with a substantial temperature gradient. The region of the Christiansen frequency is sufficiently transparent so that the radiation measured originates from depths up to 200μ for both corundum and quartz. Thus, as our measured temperature gradients ranged from 4°/cm to 40°/cm (vacuum experiments), the largest error to be expected from this effect would be about 0.8°C.

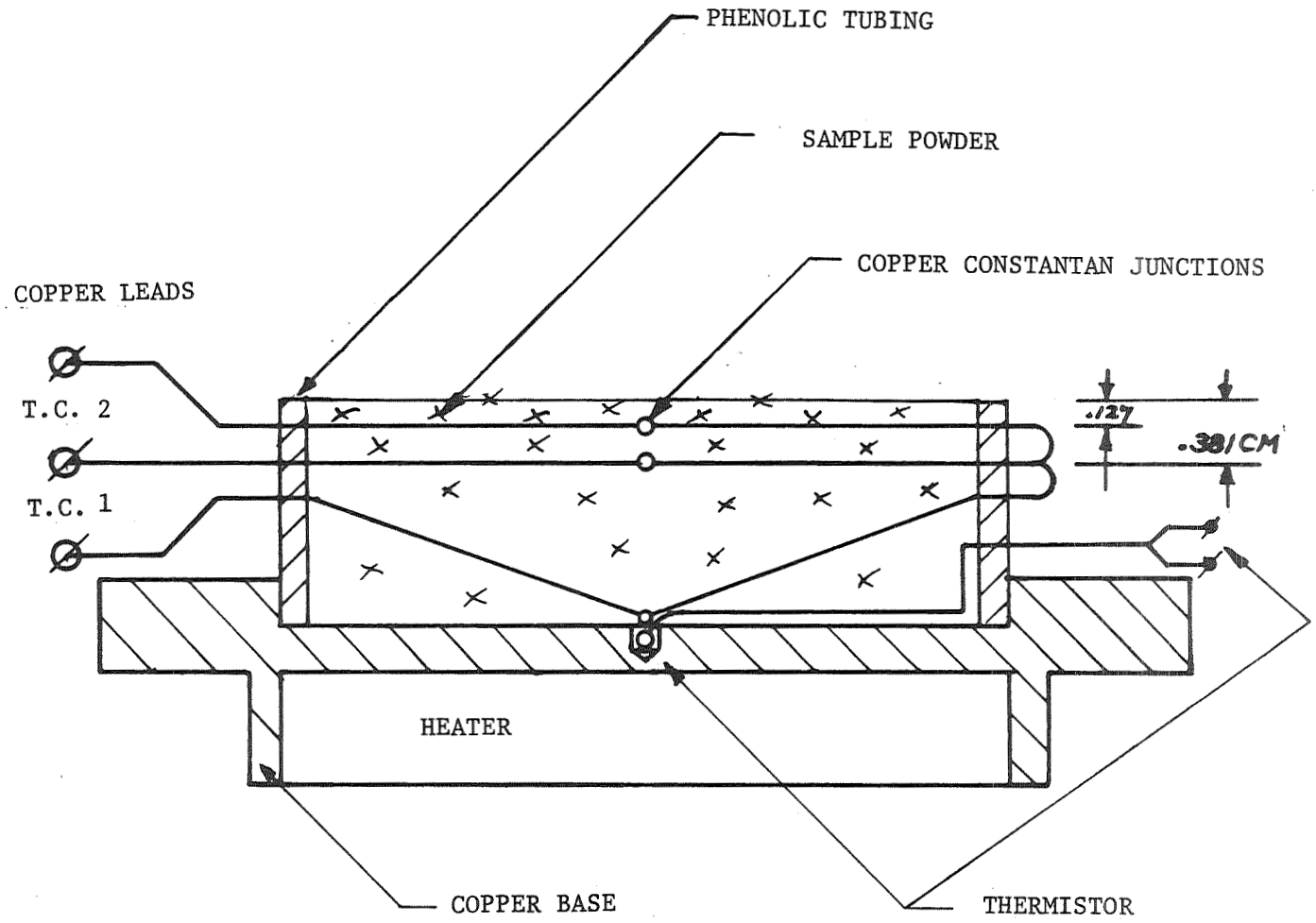

FIGURE 9. SAMPLE TRAY

IV. RESULTS

A. QUARTZ POWDERS

At the time of our most recent report[2] Dr. Warren Hovis of the Goddard Space Flight Center of NASA informed us that the fit between our theoretical curves and his experimental data was even better than shown in Figure 1. He kindly consented to make some reflectance measurements on some of our powders, using a Cary Model 90 Spectrophotometer. The data in the relevant spectral range are shown in Figure 10. Note the considerably altered spectral shape for these two samples. This will be commented on below. At the same time Dr. Hovis commented that he had run various spectra of mineral samples and certain features continued to sharpen down to resolutions of about 2 cm^{-1}. This information together with the present storage capability by our Hewlett Packard 2116B minicomputer established the resolution we have used during this year's work. Our typical runs consist of 10 coadditions and take approximately 30 minutes for the set for each sample at this resolution.

The various photographs taken of the "coarse"-quartz powders used in our previous work indicated that, as Dr. Rooney had informed us, the particle sizes were only nominal and a great many fines contaminated the supposedly coarse-particle samples. In addition, the "53μ < d < 63μ" sample contained some particles as large as 114μ. These must have passed through the sieve edgewise. Particle size distribution measurements were made on the "53μ < d < 63μ" sample and while the volume fraction of fines was quite small, a large number of them were observed (93% by number, but only 4% by volume were less than 53μ). We decided to remove the fines from these samples as follows:

Portions of the samples were agitated ultrasonically in a 1:1 ethanol-water mixture for approximately 15 minutes. After a short settling period, the particles in suspension were decanted from the material

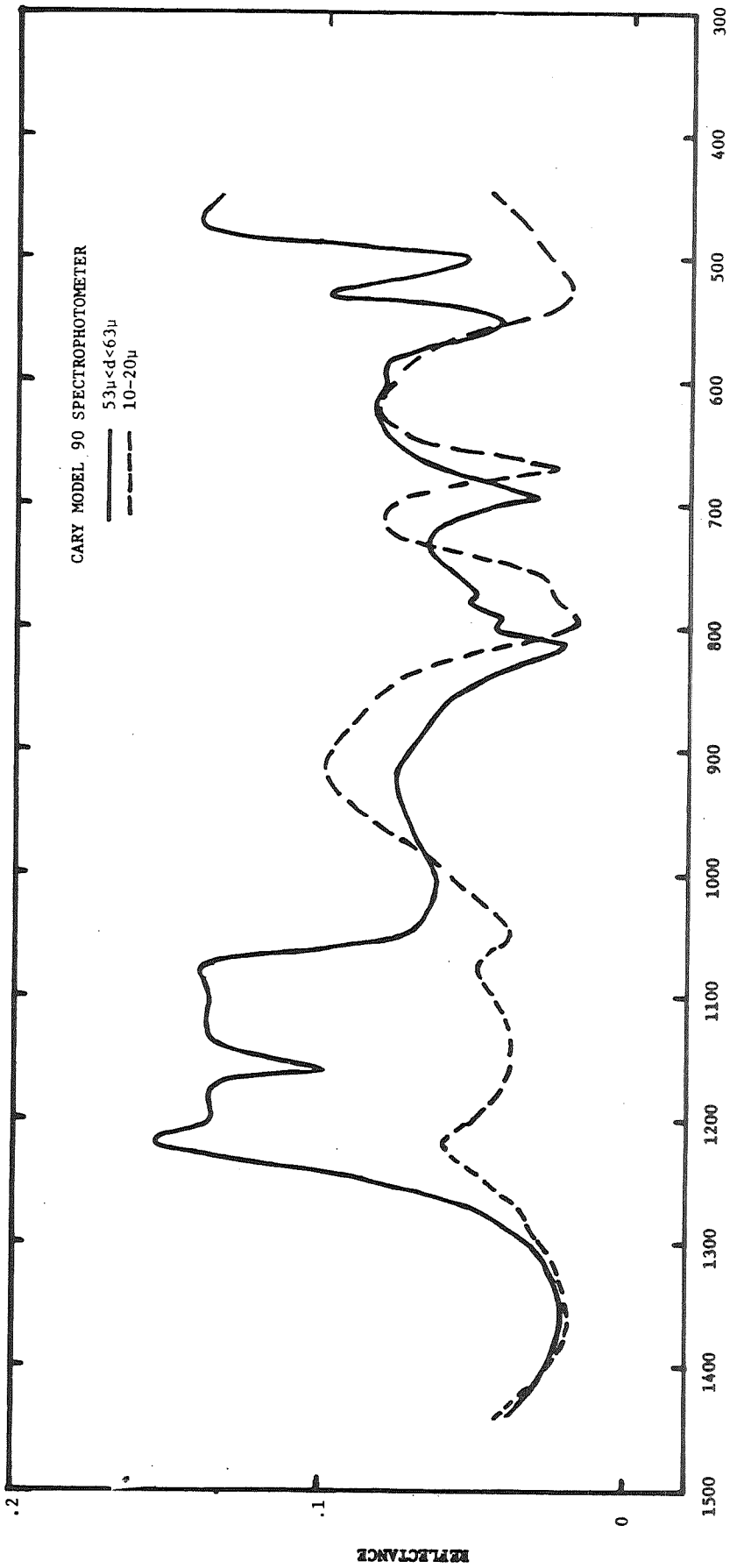

FIGURE 10. QUARTZ POWDER REFLECTANCE DATA (COURTESY OF W.A. HOVIS AND L.R. BLAINE).

that had settled to the bottom of the container. This process was repeated three or four times until agitation did not produce significant suspended material.

The residual large particles were then treated with ethanol (95%) on a sieve fabricated from two layers of silk-screen cloth. The cloth has effective openings of 55μ squares. The two layers were oriented at 45° so that the openings were 55μ at most. The sieve was vibrated during the alcohol treatment so that the smaller particles would be washed through the openings while most larger particles would be retained. The same procedure was used for several different samples of quartz powder. Usually, three or four washing cycles were sufficient to remove the fines left after the suspension treatment. Figure 11a shows the effect of this treatment. Figure 11b shows a scanning electron micrograph of the 170μ samples as they appear in our experiments.

Some of the material removed from the large particles when dried with heat showed a coloration which is assumed to be from decomposed organic material. It was noticeable that the "cleaned" particles have a much less gray coloration than do the fines or the starting material.

Our experimental results on three of the samples of coarse-quartz powders and one sample of fine-quartz powder are shown in Figure 12a. The data are shown as reflectance (1-emittance) in order to facilitate comparisons with theory. The volume fractions and particle sizes for the coarse samples were used to produce the theoretical curves shown in Figure 12b. While the particle sizes used are approximations to the actual size, the trends with particle size are clearly indicated. We have established in other theoretical runs that representing the spectrum by a dispersion of particle sizes makes only a minor difference to the theoretical results when the particles are as closely sized as these. The improvement in fit when compared with Figures 1a and 1b is apparent.

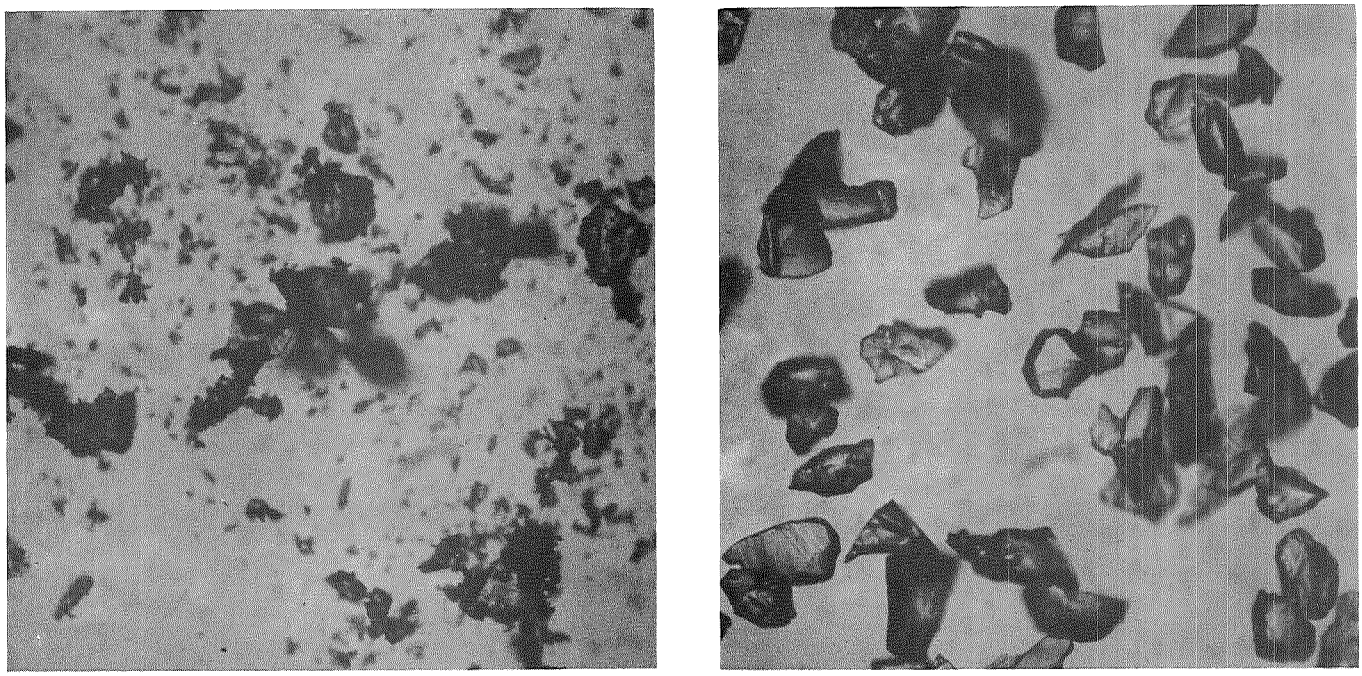

before after

a. OPTICAL MICROGRAPHS (110X) OF "53μ < d < 63μ" PARTICLES.

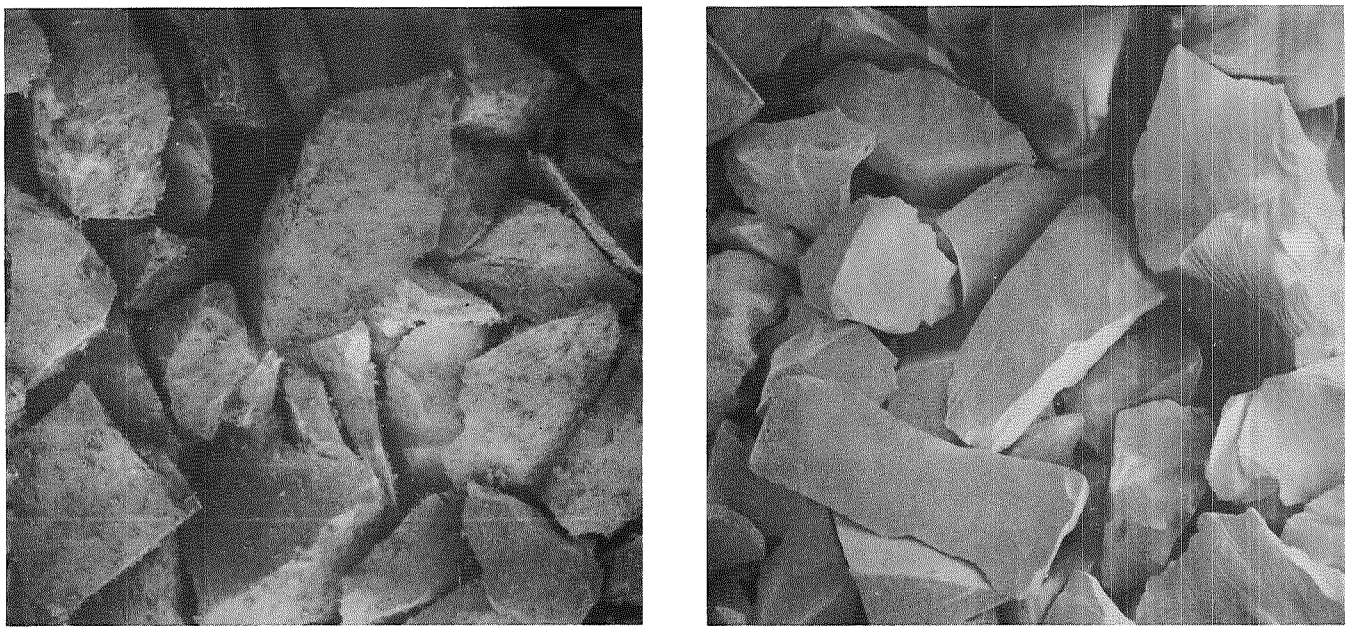

before after

b. SCANNING ELECTRON MICROGRAPHS (95X) OF "170μ" PARTICLES.

FIGURE 11. ILLUSTRATIONS OF EFFECTIVENESS OF THE REMOVAL OF QUARTZ FINES.

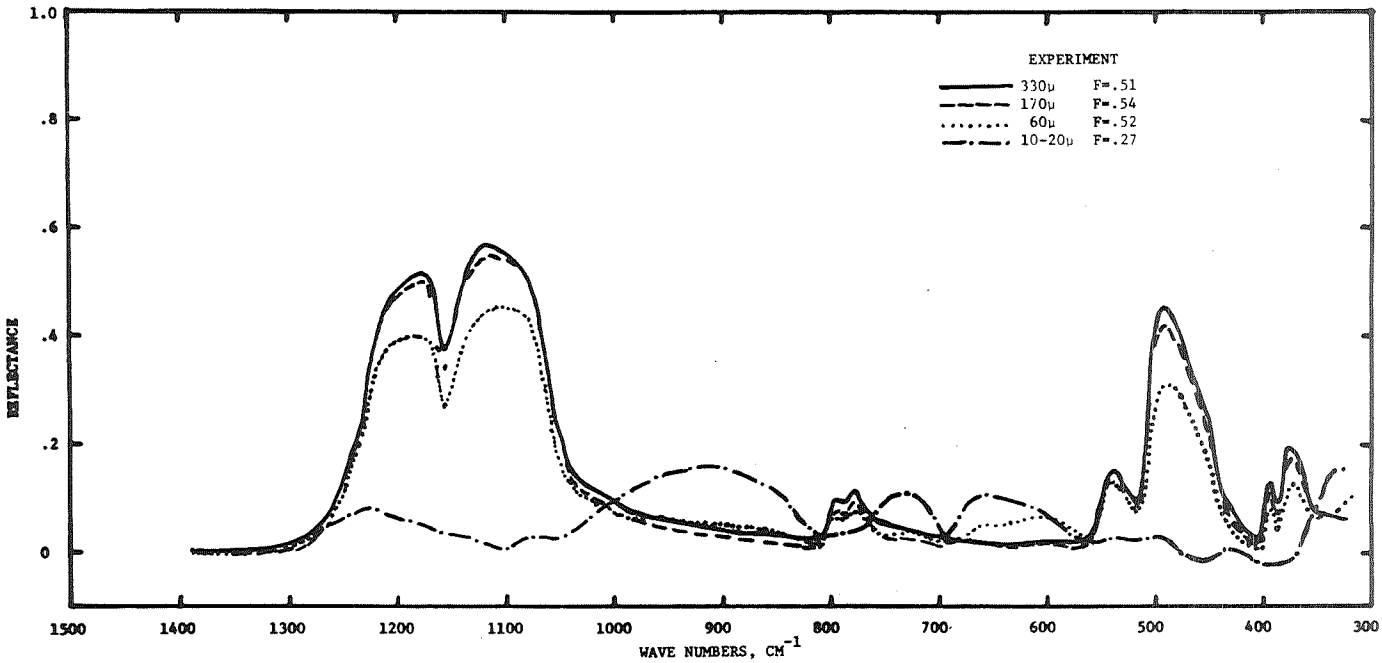

FIGURE 12a. EXPERIMENTAL REFLECTANCE OF QUARTZ POWDERS (HIGH RESOLUTION).

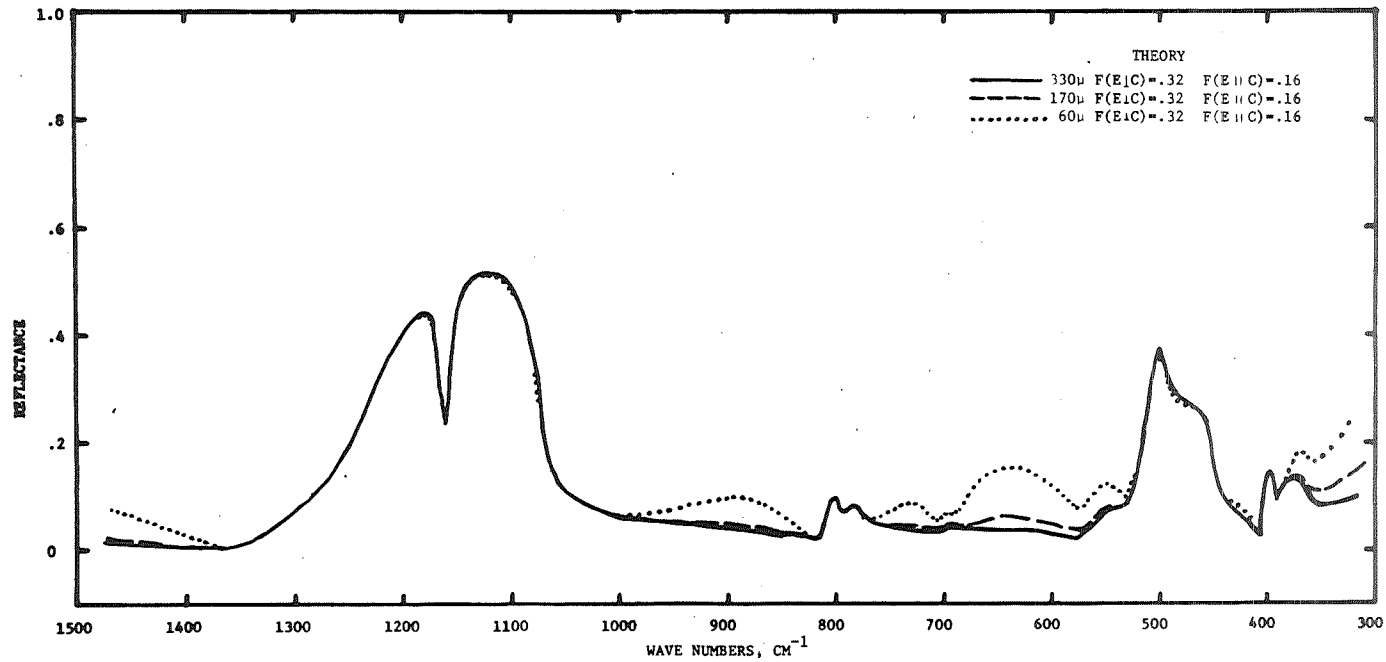

FIGURE 12b. THEORETICAL REFLECTANCE OF QUARTZ POWDERS.

Theoretical results for fine-particle sizes amplify the trends shown but do not keep pace with the experimental results.

At the same time we reran several samples of the "as received" quartz powders under the improved resolution. They are compared with the spectra of the cleaned samples in Figure 13. Certain shape changes are evident. The features particularly between 1000 cm^{-1} and 1300 cm^{-1} may be explained qualitatively by observation of a high resolution spectrum of the 10μ to 20μ quartz sample referred to previously. The particle size distribution for the latter material shows the greatest volume fraction to be centered at about 12μ, but a second peak in the distribution occurs near 19μ. The volume fraction below 4μ is negligible. While we do not consider this finer quartz sample to have a similar distribution to the removed fines, we do believe the figure is instructive. It demonstrates the large change in emittance that can result from an altered particle-size distribution when fine particles are mixed with coarse particles. The spectrum of this sample can be compared with the reflectance data obtained by Dr. Hovis and shown in Figure 10. When regard is given to the change of scale, the comparison is quite good. Figure 14 indicates that this sample shows certain features predicted from the coarse-particle theory, but at the same time has some very distinctive features. Results of the present fine-particle theory, also shown in Figure 14, indicate that there are spectral regions where the two theories are in substantial agreement, but that in other regions (1050 cm^{-1} to 1400 cm^{-1}) the fine-particle theory is required to produce a spectrum showing the same features as the data for the 10μ to 20μ sample. We have shown fine-particle theory results for a size much smaller than the actual 10μ to 20μ sample would indicate, but the appropriate size to be used in the fine-particle theory is actually a correlation distance rather than an actual particle size. We are still in the process of trying to establish the precise meaning of this distance.

It should be observed that the data for the 10μ to 20μ sample is drastically different from the coarse-particle samples in the spectral

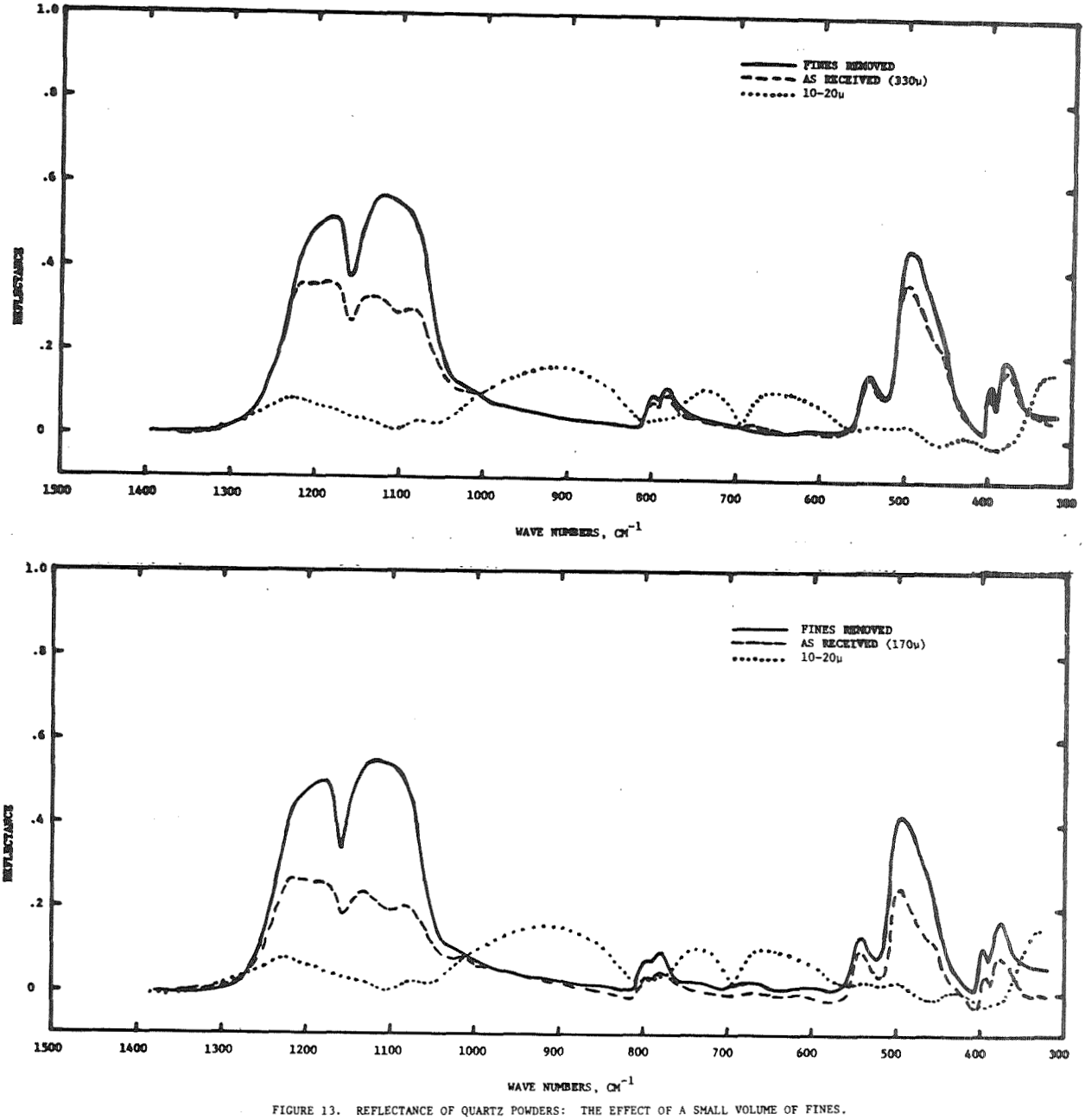

FIGURE 13. REFLECTANCE OF QUARTZ POWDERS: THE EFFECT OF A SMALL VOLUME OF FINES.

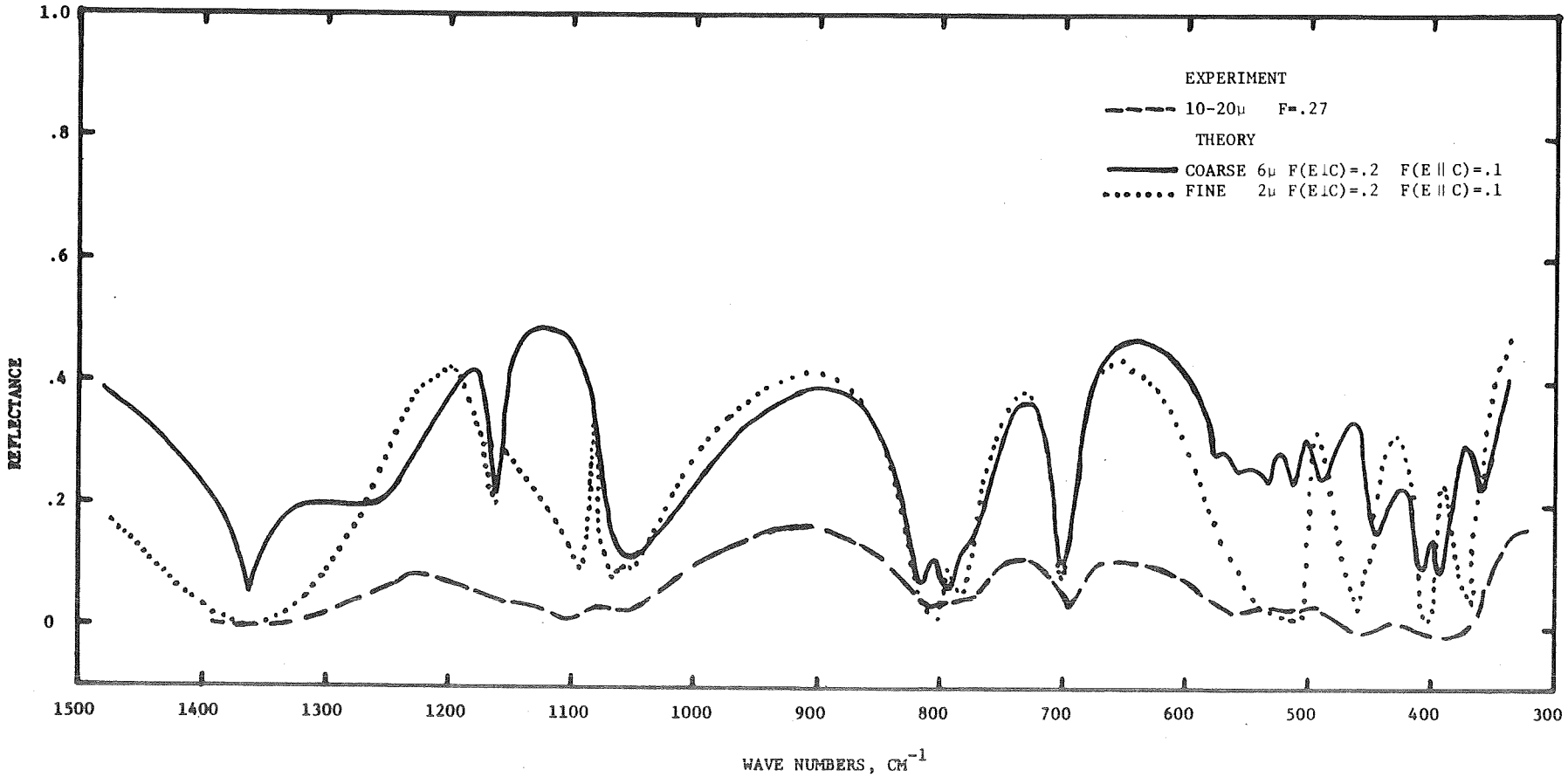

FIGURE 14. FITS TO FINE-PARTICLE QUARTZ DATA.

region between 1000 cm^{-1} and 1200 cm^{-1}. Between 1100 cm^{-1} and 1200 cm^{-1} is the region of anomalous dispersion and the refractive index n in this region falls to values near 0.1, while the absorption index k has values in the range 1 to 3. The particular shape (see Figure 10) produced in the experimental results for the 10μ to 20μ sample in this region is quite similar to what is observed for corundum in a similar region of the optical constants. We shall have more to report concerning this shape later.

1. Spectra of Quartz Powder at Reduced Pressures

During the course of this work a paper by Logan and Hunt[4] entitled "Emission Spectra of Particulate Silicates Under Simulated Lunar Conditions" was published. It reported that the emittance of powders changes substantially when measured at low pressures and in addition depends on the temperature of the background. As our new experimental apparatus can be operated under vacuum we have carried out several prelininary experiments similar to theirs. The results are shown in Figure 15. Our technique involved only warm backgrounds (∿ 23°C) and we heated the powder from beneath. As our samples were approximately 1.1-cm deep a significant temperature drop occurs across the depth of the sample. As a result of this temperature drop which was substantial in the lower pressure measurements the surface temperature reached values only about 6° above the background (cavity) and detector temperatures. Consequently, these runs had relatively small signal-to-noise ratios and some of the observed features may be spurious. Nonetheless, the results shown in Figure 15 do appear to indicate a "pressure"-dependent emittance. The magnitude of our observed effect appears to be comparable to that of Logan and Hunt. It should be noted that as with all of our other results, these curves have been reduced by setting the emittance equal to unity at the principal Christiansen frequency[3] (1360 cm^{-1} for quartz). Logan and Hunt's technique involves a similar assumption.

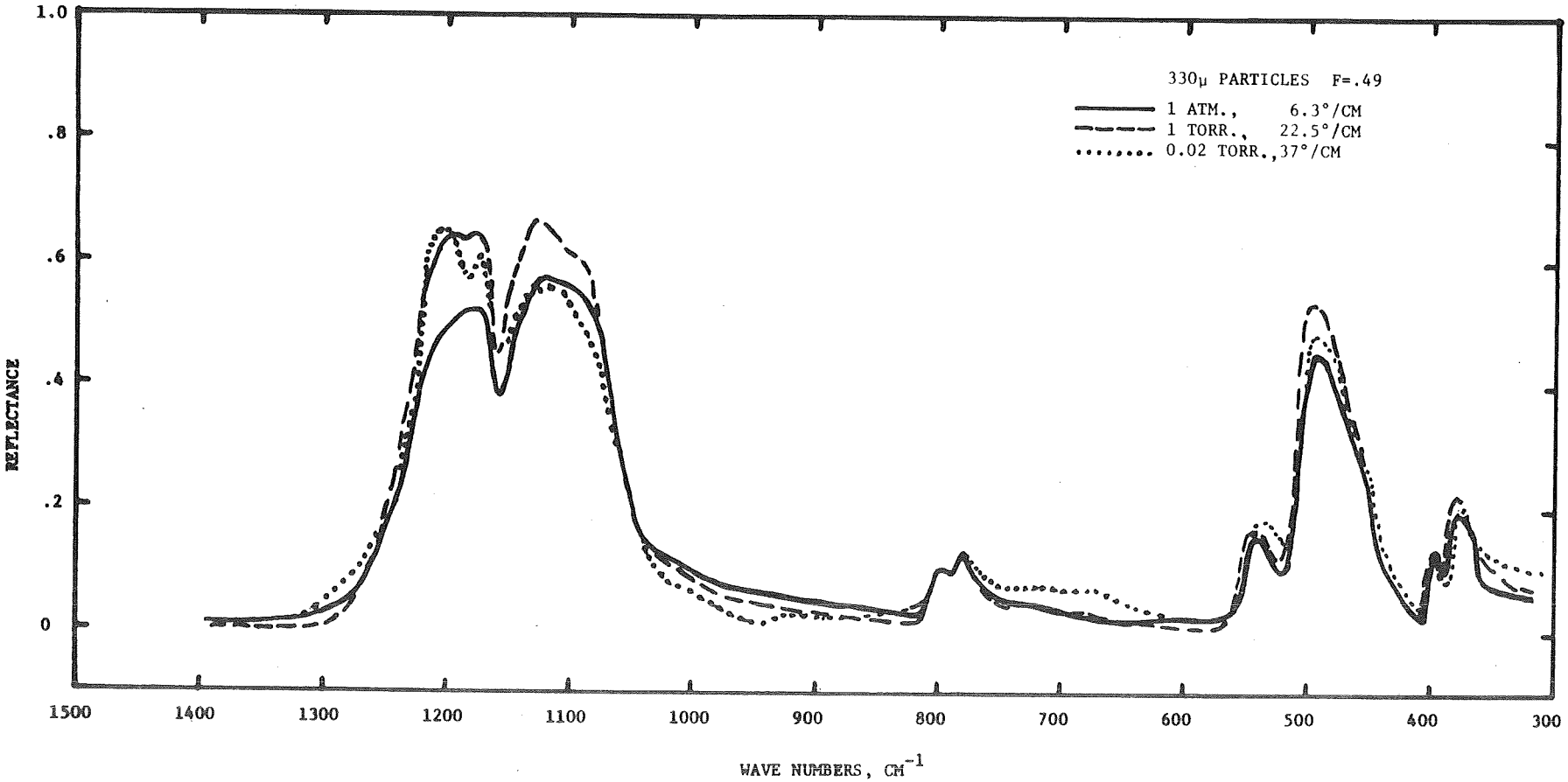

FIGURE 15. REFLECTANCE OF QUARTZ POWDERS: THE EFFECT OF AMBIENT PRESSURE.

This assumption is invalid in the case of large thermal gradients in the sample, owing to the relatively large depth of origin of the measured radiation at the Christiansen frequency. An improved procedure is to correct the emittance at each frequency for the variable depth of origin of the photons. We have derived the following formula (see Appendix B) for the correction, $\Delta\varepsilon$, to be made to the measured emittance, ε:

$$\Delta\varepsilon = \frac{(2 - \varepsilon)}{(T_s - T_b)(K + 2S)} \quad \frac{dT}{dx} \tag{28}$$

where T_s and T_b are the temperatures of the sample and the surrounding box, dT/dx is the temperature gradient at the surface of the sample, and K and S are the Kubelka-Munk parameters defined earlier.

For the case of quartz at its Christiansen frequency we calculate that $\Delta\varepsilon = 0.21$; at 1200 cm^{-1} the calculation yields $\Delta\varepsilon = 0.15$. Thus an error in the relative values at these two points is incurred. At atmospheric pressure where the gradient is substantially less (see Figure 15) the calculation gives $\Delta\varepsilon \approx 0.01$ at both frequencies. The value of K + 2S taken from our theoretical computations is 29.2 cm^{-1} at 1360 cm^{-1} and 41.2 at 1200 cm^{-1}. We believe that when these considerations are incorporated into our existing data reduction procedure and when the data for low pressures are run at better signal-to-noise ratios, the apparent emittance differences observed will disappear.

In the case of a mixture of minerals such as occurs in most powdered rocks, the entire concept of a Christiansen frequency is invalid. As n is very unlikely to pass through unity (while k is small) at the same frequency for the different components, no principal Christiansen frequency can be expected. The highest radiance position in the spectrum is thus not a point of unit emittance as assumed by Logan and Hunt.[4]

2. Comparison of Coarse-Particle Theory with Mie Theory

It is of interest to check our relatively simple geometrical optics theory for coarse particles against the predictions of the much more complicated Mie theory for large spherical particles. For this purpose we use the Mie theory calculations of J. E. Conel[5] of the emittance of a cloud of quartz spheres. In his calculations the optical constants were assumed to be those of the E $\perp$ C orientation of quartz taken from Spitzer and Kleinman.[6] Figure 16 shows a comparison of Conel's theoretical results with computer runs using our coarse-particle theory and the same optical constants. In the case of a cloud our contact factor automatically goes to unity since the volume fraction of the particles tends to zero.

We see that excellent agreement is obtained for the larger particle sizes and surprisingly good agreement down to particle sizes as small as 12μ (note the ordinates are on different scales). This proves that our random interface model for coarse particles is valid for scattering by clouds as well as by powders. The computational simplicity of the random interface model, its applicability to particles of any shape, and its validity for both clouds and powders (on account of the contact factor) appear to make this theory preferable to the Mie theory at least for particles that are moderately large compared with the wavelength.

B. CORUNDUM POWDERS

As stated in the Introduction, our previous work had led us to believe that the fine-particle theory accounted for much of the corundum spectrum. However, during the current contract we obtained a number of coarser samples and ran these in an effort to explore the changeover into the coarse-particle region. These samples were chosen so as to remove any questions concerning the peculiar geometry of the WCA powders previously studied. The Microabrasives Corporation supplied us with a number of their LWA optical finishing powders which are reported[7] to be

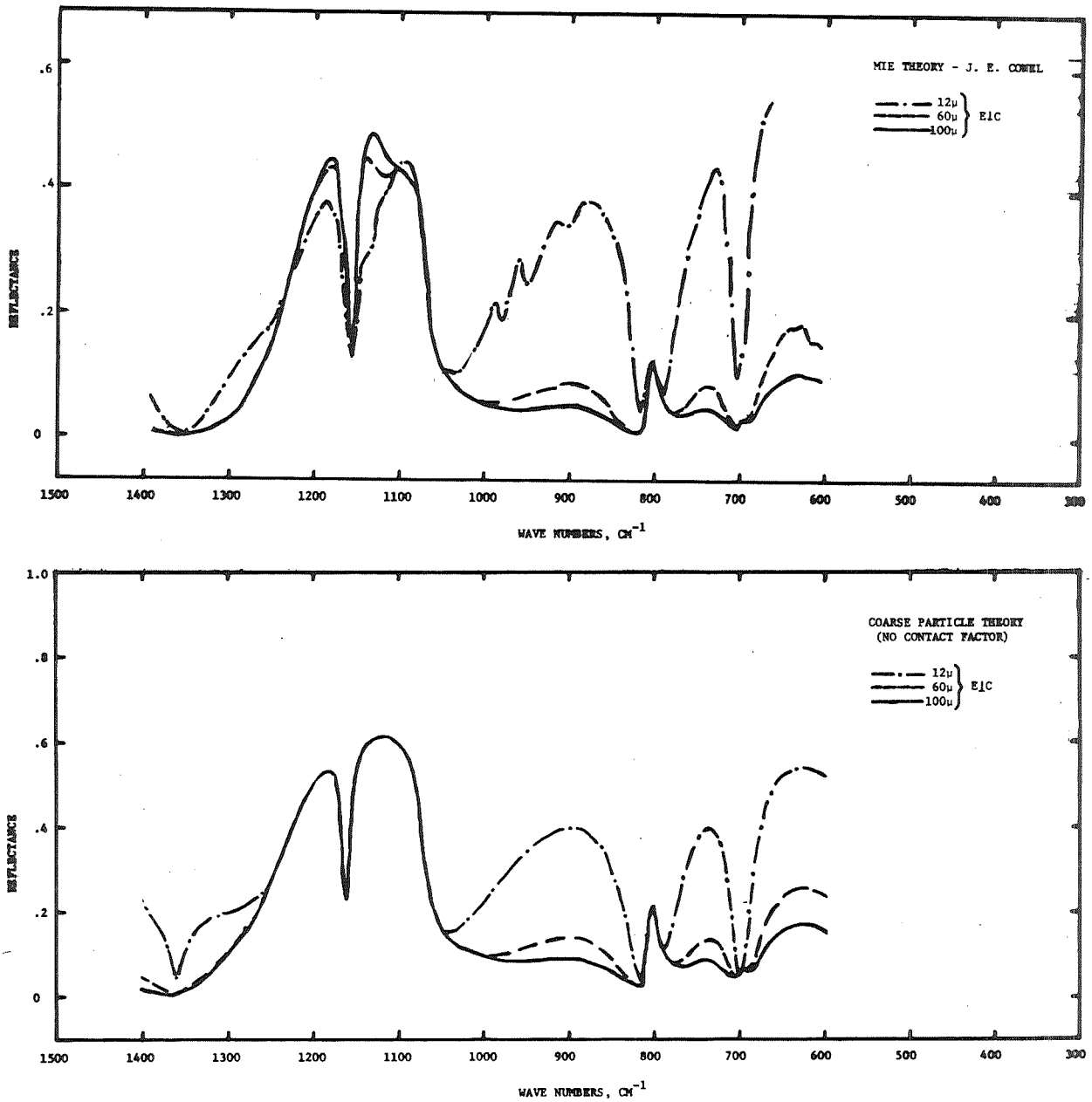

FIGURE 16. COMPARISON OF THE COARSE-PARTICLE THEORY AND MIE THEORY.

99.5% α-Al_2O_3. The Norton Company provided us with a relatively coarse sample (122μ) No. 38 Alundum. They report a purity of 99.55%. These powders, manufactured by different processes than the WCA powders, do not have the platelet shape, but appear to be more chunky. As with most abrasive powders they are crushed from larger pieces and do not necessarily represent individual crystallites. Figure 17 shows a typical particle. Runs on 10μ, 60μ, and 122μ corundum are shown in Figure 18a, along with a rerun of the coarsest corundum powder studied in our previous work.

At the same time theoretical spectra of corundum powders have been examined and while both theories appear to produce some of the features observed in our experiment, neither theory nor any obvious combination of them produces the shape of the curve in the spectral region between 650 cm^{-1} and 860 cm^{-1}. Outside of this region the fit using the coarse-particle theory (Figure 18b) appears to be quite satisfactory except that the particle-size dependence at frequencies less than 1000 cm^{-1} is much too slow. Part of the improvement of the fit for this material results from the new coarse-particle theory but some of the credit must go to the use of a different set of oscillator parameters, and hence, optical constants, used in the fitting.

Corundum is an unusual material in that various surface treatments can alter the spectrum to a certain extent. Barker[8] studied these effects and concluded that the changes in the spectrum were due to the relaxation of the normal selection rules when the surface was strained by various grinding techniques. He gave oscillator parameters for undisturbed (4 oscillators) and disturbed surfaces (6 oscillators) for the E⊥C orientation of corundum. As small particles might be expected to be strained in crushing we have generally used his oscillator parameters (optical constants) for the disturbed surface, although early in our work, both sets were tried. With the current theory, the oscillator parameters for an undisturbed surface appear to give a superior fit and so those are now being used.

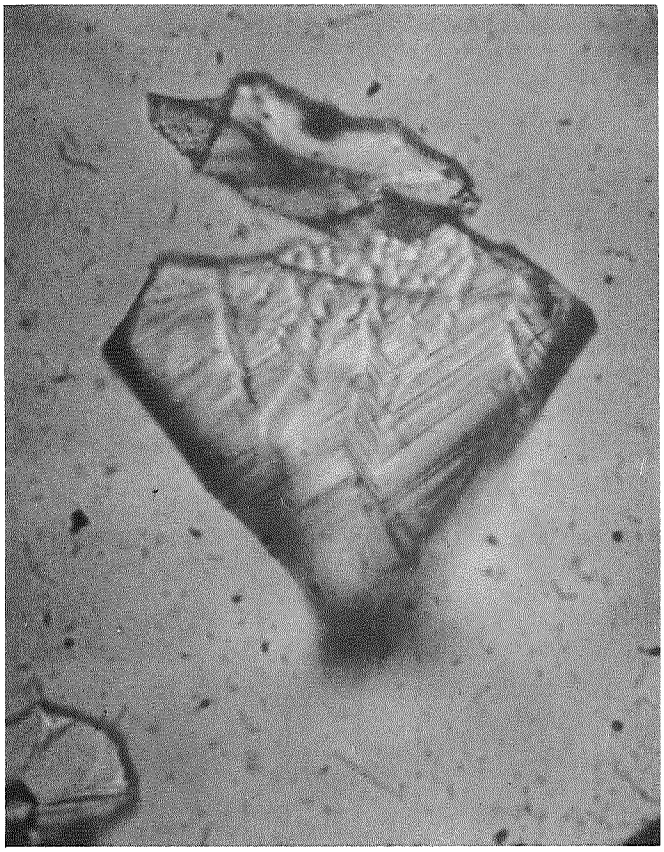

FIGURE 17. A TYPICAL LARGE CORUNDUM PARTICLES (500X).

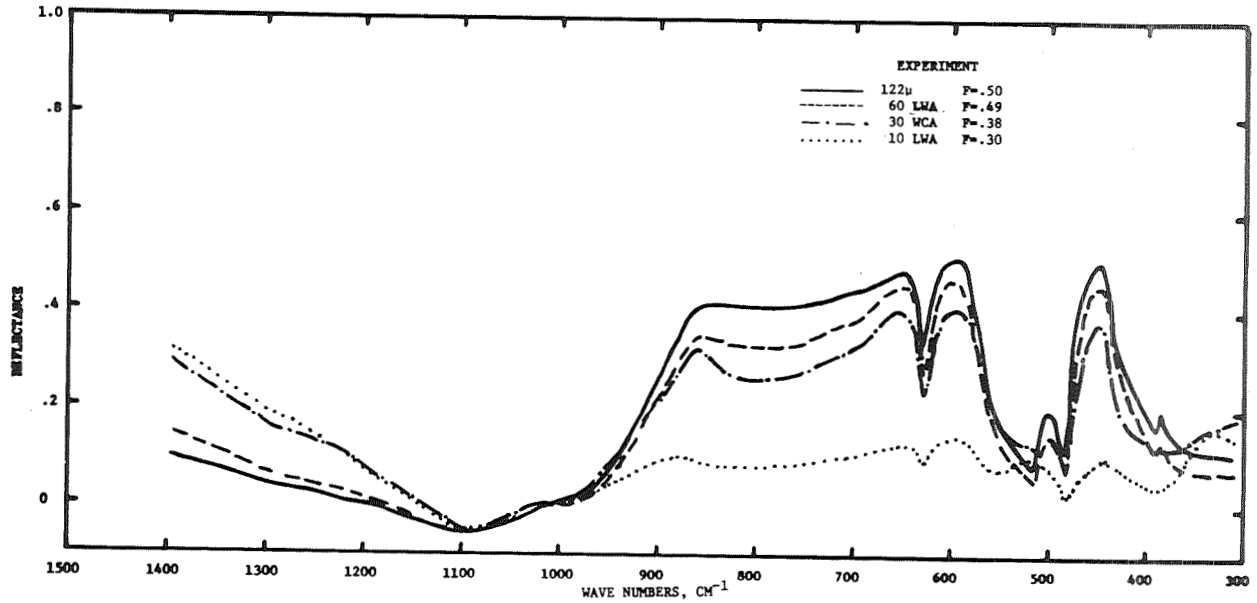

FIGURE 18a. EXPERIMENTAL REFLECTANCE OF CORUNDUM POWDERS.

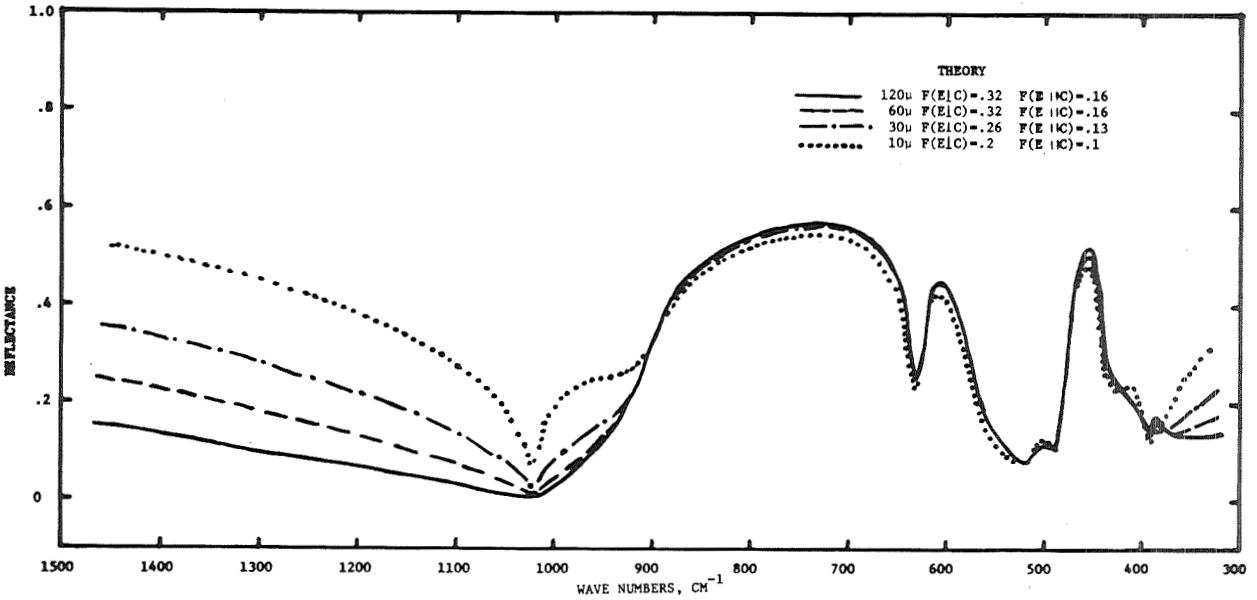

FIGURE 18b. THEORETICAL REFLECTANCE OF CORUNDUM POWDERS.

As stated previously, the region between 650 cm^{-1} and 860 cm^{-1} is our principal source of difficulty. The Lorentz-Lorenz theory predicted the proper trend in this region (Figure 2b), providing the surface terms were not used, but produced too great an effect. However, the present fine-particle model (results not shown) with its accounting for skin depth, while retaining the general shape of the Lorentz-Lorenz theory results in the region between 1000 cm^{-1} and 800 cm^{-1}, does not appear capable of producing the reflectance rise experimentally observed with decreasing frequency in the region between 800 cm^{-1} and 650 cm^{-1} (Figure 18a). At the same time the coarse-particle theory (Figure 18b) produces a shape in this region that essentially mimics the shape of single crystal spectra. The experimental shape in this region, which appears to be a "scallop" taken out of the coarse-particle-model theory, appears to slowly change as coarser particles sizes are reached. However, even the 122μ particles show its presence. The curve also appears to flatten at smaller particle sizes. These results force us to conclude the effect is not a simple fine-particle effect. The region of this difficulty is the region of anomalous dispersion where n drops to values near 0.1 and k is quite large. This is a similar spectral region to that where fine quartz showed a similar feature (Figure 10).

We have considered various possible explanations for the scallop phenomenon, including:

a. Waveguide effects
b. Birefringence effects
c. Altered optical constants
d. Surface disturbances
e. Independent dipole scattering

1. Waveguide Propagation

For $n \ll 1$ the radiation tends to be strongly concentrated in the voids rather than in the particles, owing to the effect of near total

external reflection. For example, if m = n = 0.1, radiation has to be directed within an angle of 6° to the normal to a particle surface to enter the particle. Propagation in a channel between particles is closely analogous to the propagation of light in a light pipe. The wave in the channel is however attenuated to a degree that depends on the absorption index k of the walls of the channel, owing to the presence of an evanescent part of the wave in the walls.

The nature of the waveguide propagation is most easily understood for scalar waves which satisfy the wave equation

$$\nabla^2\phi + m_p^2 K_o^2 \phi = 0 \tag{29}$$

in the walls (i.e., particles) of the waveguide, where m is the complex index of the particles. The same equation with $m_p = 1$ applies in the channels. For simplicity, we consider a channel of width g between infinite walls. Let x be in the direction of propagation and y at right angles to the walls. Then we can take as solutions in the two regions

$$\phi = Ae^{iK_1 x} \cos K_2 y \quad , \quad y \leq \frac{g}{2} \tag{30}$$

$$\phi = Be^{iK_1 x} e^{-\alpha y} \quad , \quad y \geq \frac{g}{2} \tag{31}$$

To satisfy (29), K_1, K_2, and α must satisfy the relations

$$K_1^2 + K_2^2 = K_o^2 \tag{32}$$

$$K_1^2 - \alpha^2 = m_p^2 K_o^2 \tag{33}$$

Also ϕ and $\frac{\partial\phi}{\partial y}$ must be continuous at $y = \frac{g}{2}$ (the wall of the waveguide). Therefore

$$A \cos\left(\frac{K_2 g}{2}\right) = B\, e^{-\frac{\alpha g}{2}} \tag{34}$$

$$K_2 A \sin\left(\frac{K_2 g}{2}\right) = \alpha B\, e^{-\frac{\alpha g}{2}} \tag{35}$$

From (34) and (35) we find that

$$K_2 \tan\left(\frac{K_2 g}{2}\right) = \alpha \tag{36}$$

From (32), (33), and (36) we obtain, on eliminating K_2 and α,

$$\frac{\sqrt{K_o^2 - K_1^2}}{\cos\left(\frac{g}{2}\sqrt{K_o^2 - K_1^2}\right)} = K_o\sqrt{1 - m_p^2} \tag{37}$$

We can define the waveguide complex refractive index m by the equation

$$m = \frac{K_1}{K_o} \tag{38}$$

Then (38) becomes, with $K_o = 2\pi\nu$:

$$\frac{\sqrt{1 - m^2}}{\cos\left(\pi g \nu \sqrt{1 - m^2}\right)} = \sqrt{1 - m_p^2} \tag{39}$$

For given values of m_p, g, and ν this multivalued equation can be solved for the waveguide index m for each of the allowed waveguide modes. Figures 19 and 20 show the real and imaginary parts n and k for the lowest waveguide mode in corundum powder for various assumed gap widths.

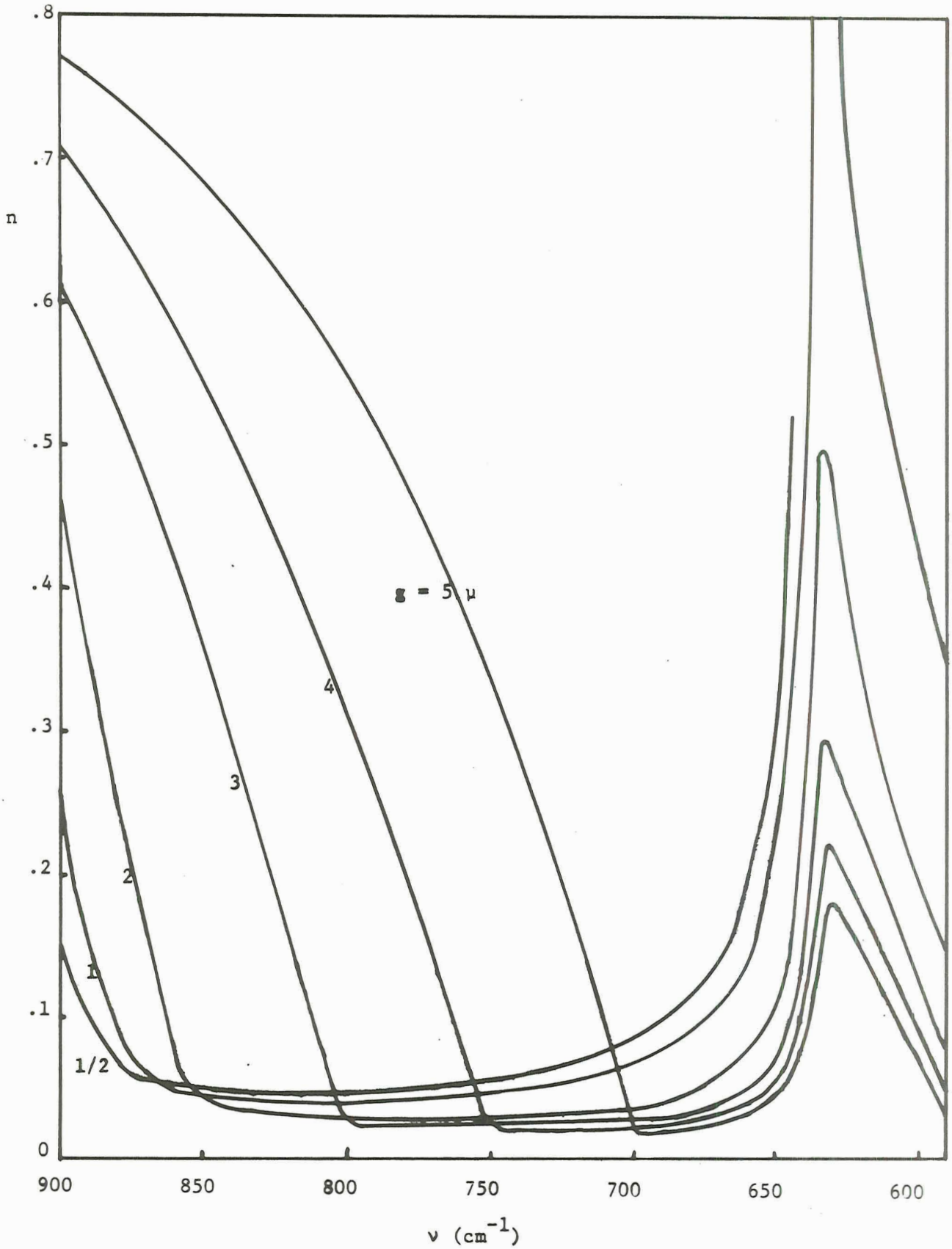

FIGURE 19. WAVEGUIDE REFRACTIVE INDEX FOR THE LOWEST TE MODE.

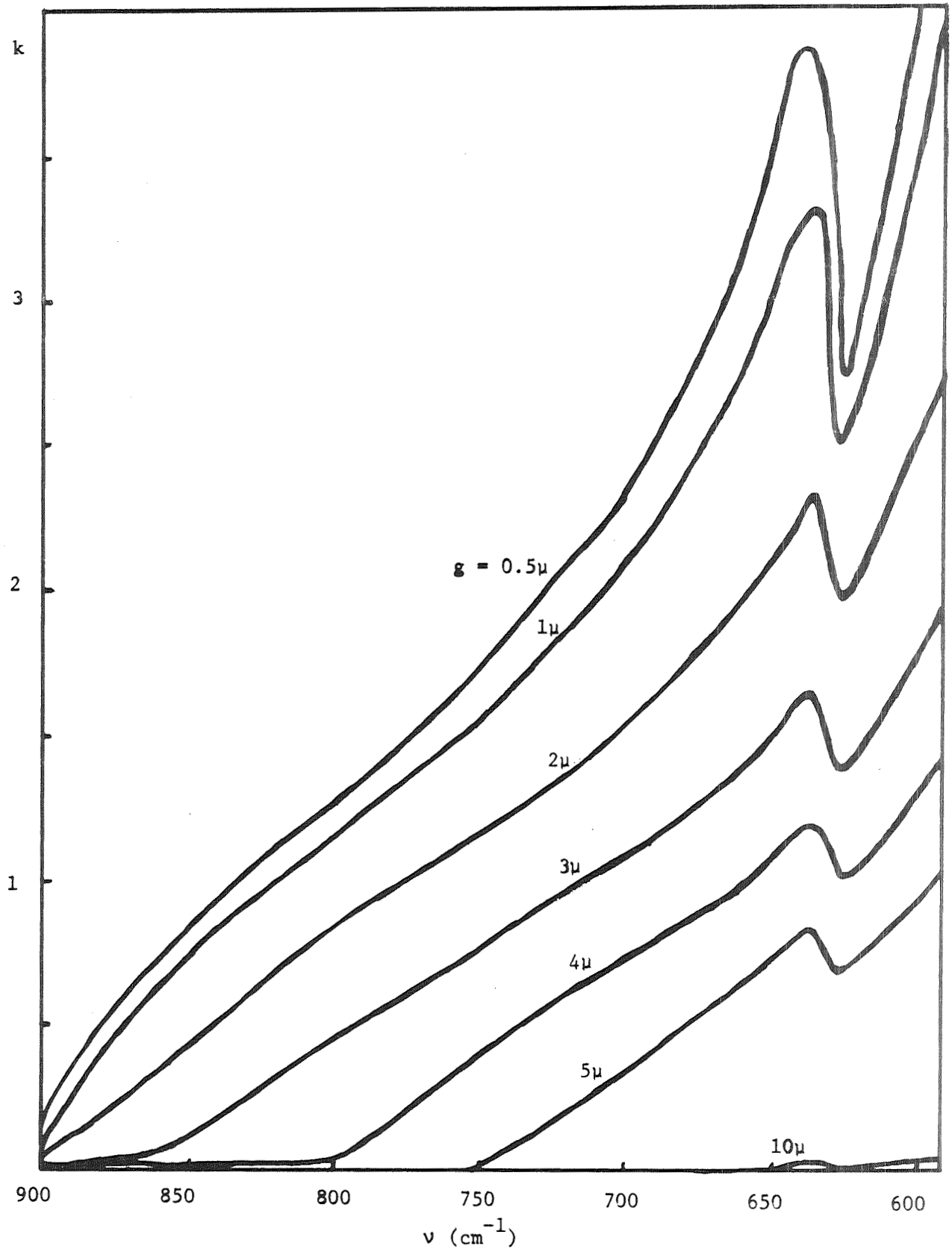

FIGURE 20. WAVEGUIDE ABSORPTION INDEX FOR THE LOWEST TE MODE.

The trend of the waveguide absorption index with frequency is similar to that of the single crystal absorption index. The effect of this trend is to add to the ordinary K of the powder a waveguide contribution that increases steadily with decreasing frequency. This results in a similar trend in the reflectance and does not produce a scallop.

The variation of waveguide refractive index with frequency, when averaged over gap width, is in general like that of the single crystal index with a minimum of the index within the frequency range of interest. The effect on reflectance is therefore also to give a maximum in the region of the scallop. The combined effect of the waveguide n and k merely shifts the single crystal reflection maximum and does not lead to a scallop.

For electromagnetic waves one obtains exactly the same results as for scalar waves when the electric field is parallel to the walls of the waveguide (TE modes). With the magnetic field parallel to the walls (TM modes), Eq (39) is replaced by the more complicated equation:

$$\frac{\sqrt{1 - m^2}}{\cos\left(\pi g \nu \sqrt{1 - m^2}\right)} = \sqrt{\frac{(1 - m_p^2)}{m_p^4} + \left(1 - \frac{1}{m_p^4}\right)(1 - m^2)} \qquad (40)$$

It is to be noted that m^2 and m_p^2 cannot be separated as in (39). This greatly increases the difficulty of computing m^2, for given values of the other parameters, owing to branch jumping in the application of Newton's method. We have not succeeded in overcoming this difficulty and therefore do not have curves of n and k for the lowest TM mode. However, it does not appear to be very likely that the results would differ significantly from the results for scalar waves and TE waves.

In order to examine the waveguide concept experimentally, we chose to run the emittance spectrum of a "monolayer" of corundum particles. The procedure was to prepare a monolayer having sufficient coverage to get an acceptable signal, yet that would be sparse enough to minimize particle-particle contacts and therefore waveguide effects. For the purposes of this experiment an aluminum disc was blackened on one side and two-sided masking tape attached to the other side. Particles from the 122μ sample were allowed to fall on this surface until the above criteria appeared to be met. A photograph is shown in Figure 21. The spectrum is shown in Figure 22. It was obtained using an identical masking tape covered disc as a reference. The two discs were simply placed on our two blackbody sources which were run at approximately the same temperature (39°C). The data was processed as in our previous calibration technique as we had found no errors in the spectral region of the "scallop." As the particles are quite opaque in this spectral region for this particle size and as the masking tape appears to produce a good facsimile of a blackbody spectrum, the result of this experiment is that a "monolayer" of particles does retain the scallop feature. While some particle-particle contacts inevitably do occur, we feel that the explanation of the scallop is to be found elsewhere.

2. Effect of Birefringence

The single crystal reflectance spectra,[8] which show no scallop effect, were obtained at near normal incidence with the electric field either parallel or perpendicular to the optic axis of the uniaxial crystal (c-axis). In the case of powders where the radiation is diffuse, the electric field is in general at an arbitrary angle to the c-axis of any crystallite. We therefore wondered whether interference effects involving the two optical constants $m_{\parallel}$ and $m_{\perp}$ could give rise to the scallop.

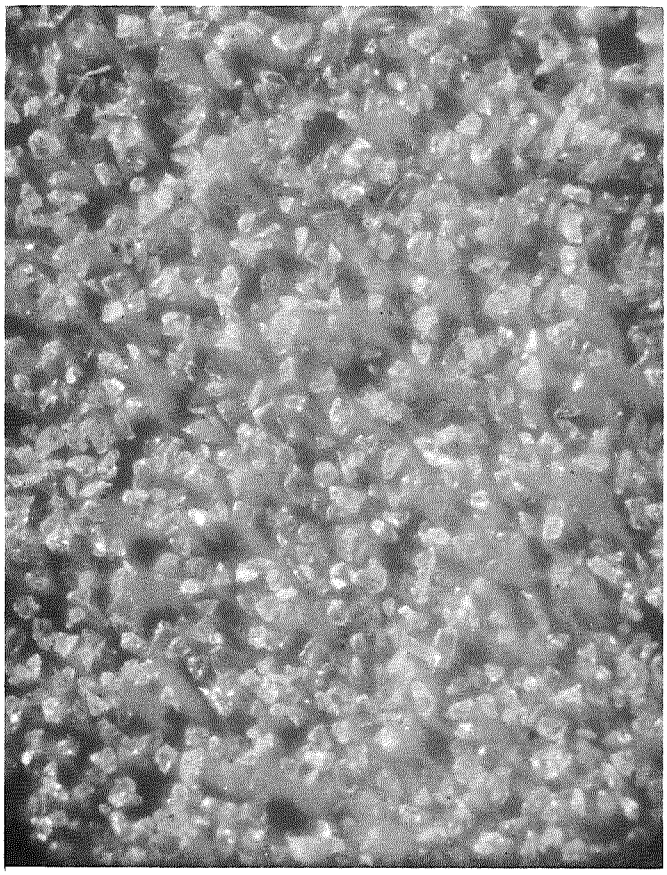

FIGURE 21. MONOLAYER OF CORUNDUM PARTICLES.

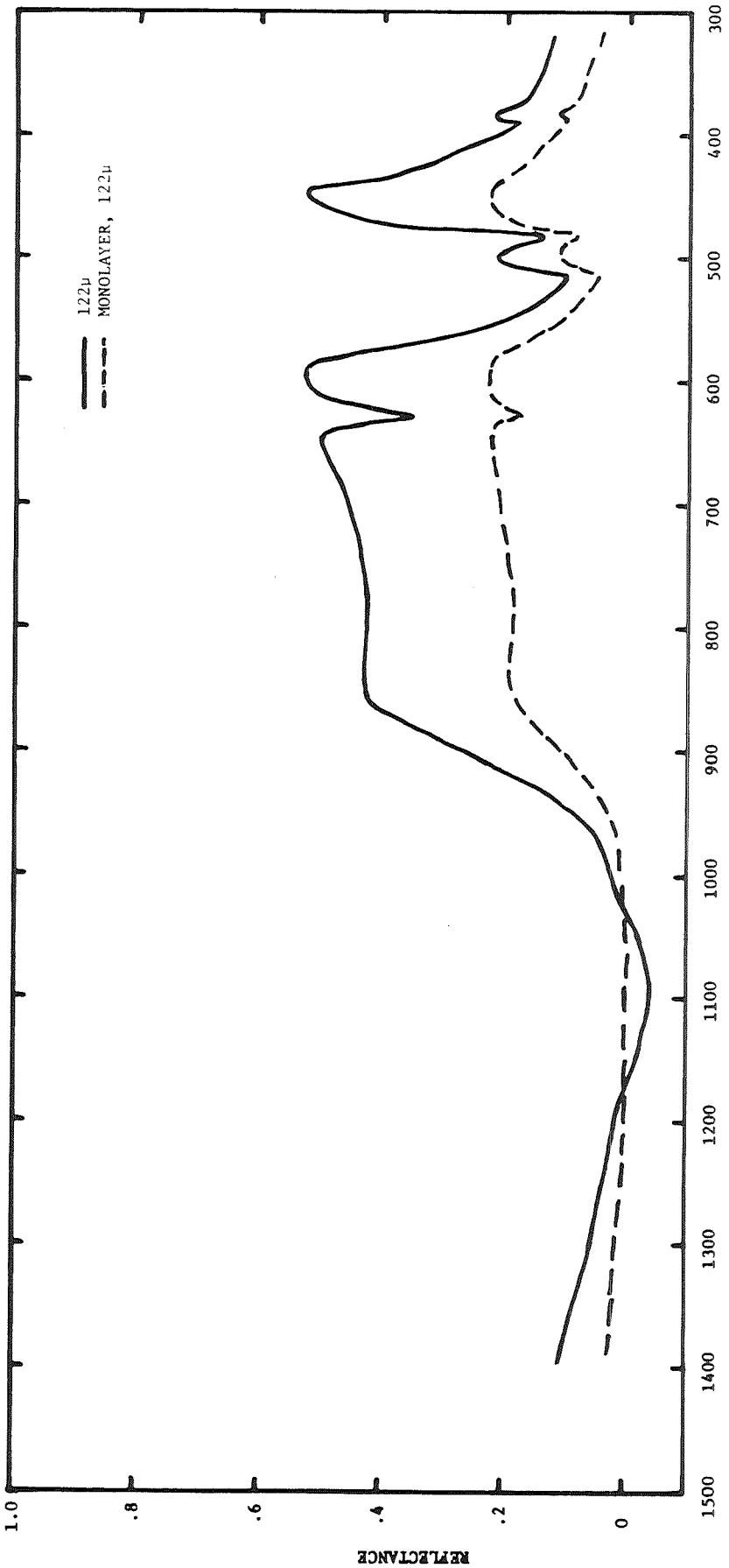

FIGURE 22. REFLECTANCE OF A MONOLAYER OF CORUNDUM PARTICLES.

The general case in which the c-axis is at an arbitrary angle to a crystal facet and to the plane of incidence is very complicated. We therefore undertook to examine the six special cases shown in Table I in which the c-axis is either parallel or perpendicular to the crystal facet and is either in or perpendicular to the plane of incidence, and where both polarizations of the incident radiation are considered. The Fresnel formulae for the six cases can be derived by the usual methods and are shown in the diagram. It is to be noted that only in the first two cases, where the electric field E is inclined to the c-axis at an angle other than 0° or 90° is there any mixing of the two indices $m_{\parallel}$ and $m_{\perp}$.

We have computed the reflectance R for an angle of incidence $\theta = 45°$ over the spectral range of the scallop for each of the six cases. The results all show a pronounced peak, similar to the measured normal incidence peak, with no sign of a scallop.

TABLE I

REFLECTANCE (R) FOR VARIOUS ORIENTATIONS OF C-AXIS AND ELECTRIC FIELD (E)

TM WAVES

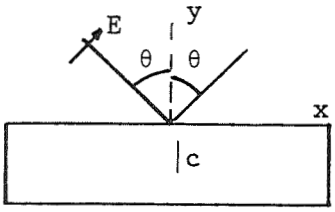

c∥y

$$R_{c\parallel y} = \left| \frac{m_\perp \cos\theta - \sqrt{1 - \frac{1}{m_\parallel^2}\sin^2\theta}}{m_\perp \cos\theta + \sqrt{1 - \frac{1}{m_\parallel^2}\sin^2\theta}} \right|^2$$

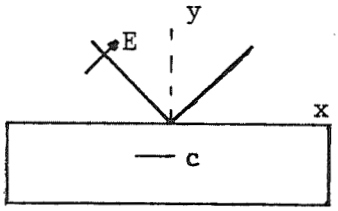

c∥x

$$R_{c\parallel x} = \left| \frac{m_\parallel \cos\theta - \sqrt{1 - \frac{1}{m_\perp^2}\sin^2\theta}}{m_\parallel \cos\theta + \sqrt{1 - \frac{1}{m_\perp^2}\sin^2\theta}} \right|^2$$

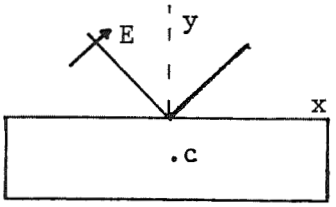

c∥z

$$R_{c\parallel z} = \left| \frac{m_\perp \cos\theta - \sqrt{1 - \frac{1}{m_\perp^2}\sin^2\theta}}{m_\perp \cos\theta + \sqrt{1 - \frac{1}{m_\perp^2}\sin^2\theta}} \right|^2$$

TE WAVES

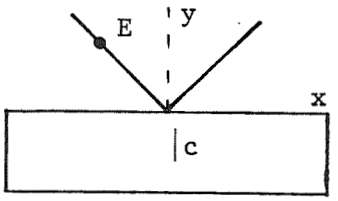

c∥y

$$R_{c\parallel y} = \left| \frac{\frac{\cos\theta}{m_\perp} - \sqrt{1 - \frac{1}{m_\perp^2}\sin^2\theta}}{\frac{\cos\theta}{m_\perp} + \sqrt{1 - \frac{1}{m_\perp^2}\sin^2\theta}} \right|^2$$

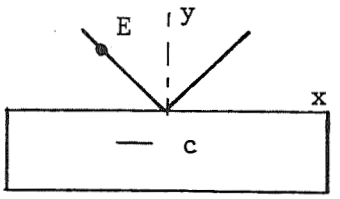

c∥x

$$R_{c\parallel x} = \left| \frac{\frac{\cos\theta}{m_\perp} - \sqrt{1 - \frac{1}{m_\perp^2}\sin^2\theta}}{\frac{\cos\theta}{m_\perp} + \sqrt{1 - \frac{1}{m_\perp^2}\sin^2\theta}} \right|^2$$

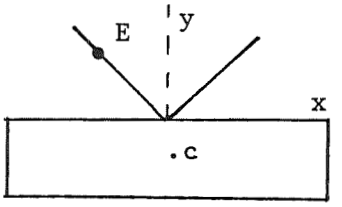

c∥z

$$R_{c\parallel z} = \left| \frac{\frac{\cos\theta}{m_\parallel} - \sqrt{1 - \frac{1}{m_\parallel^2}\sin^2\theta}}{\frac{\cos\theta}{m_\parallel} + \sqrt{1 - \frac{1}{m_\parallel^2}\sin^2\theta}} \right|^2$$

3. Altered Optical Constants

We have referred above to the experiments of Barker[8] where abrasion of the surface of a single crystal appears to introduce extra resonances in the dispersion formula of the crystal. This effect does not seem to be responsible for the scallop, and Barker's modified dispersion formula would cause alteration of the spectrum in regions other than the $n << 1$ region of interest here. Such alteration is not observed in our corundum spectra.

However, it is still conceivable that the optical constants of small particles are intrinsically different from those of a large single crystal. For example, the curvature of the surfaces of the particles, the effect of self-abrasion of the particles, or a change in the phonon spectrum due to the finite volume of the particle could be responsible for differences.

It is also possible that Barker's optical constants are not precisely correct in the region of the scallop because of problems of fitting the spectral measurements in this region. We have noted in a report by Phillippi[9] that a feature resembling the scallop is produced by using a different set of optical constants for corundum. He used data[10] that showed a different curvature for the refractive index in the spectral region of the very low values. The scale on the original data and the method used to obtain it suggest that the curvature in this region is uncertain. Nonetheless, if these values are correct rather than those given by Barker's treatment, a scallop could be produced.

4. Surface Disturbances

Under conditions of near-total external reflection ($n << 1$) the radiation field in a particle consists of a wave propagating parallel to

the surface and decreasing exponentially in amplitude with distance into the particle. The depth of penetration of this evanescent wave is, in general, a small fraction of the free space wavelength. Therefore the wave is very sensitive to disturbances such as roughness, fissures, inclusions, etc. Figure 17 shows a photomicrograph of a particle of 122μ corundum. Such disturbances are clearly visible and appear to be related to cleavage planes. Scattering of the evanescent wave by these disturbances can project a portion of the wave energy farther into the particle where it is absorbed. The effect is to lower the reflectance of the surface.

Since the depth of penetration of the evanescent wave is very small when n is close to zero, the loss of energy due to surface disturbances will be greatest for such values of n. It is significant that the reflectance minimum in the region of the scallop coincides with the minimum value of n.

5. Independent Dipole Scattering

A final possible approach to the scallop problem is to treat the particles as a set of Lorentz dipoles scattering independently of each other. This approximation assumes that each particle is small enough that the induced electric field is essentially uniform throughout the volume of the particle and that the particles are far enough apart so that they can be treated as independent scatterers.

According to the Lorentz theory, the total scattering and absorption cross-sections for a single spherical particle of index m and radius a are[11]

$$\sigma_s = \frac{8}{3} (\pi a^2) \left(\frac{2\pi a}{\lambda}\right)^4 \left| \frac{m^2 - 1}{m^2 + 2} \right|^2 \qquad (41)$$

$$\sigma_a = -4(\pi a^2)\left(\frac{2\pi a}{\lambda}\right) \mathrm{Im}\left(\frac{m^2 - 1}{m^2 + 2}\right)^2 \qquad (42)$$

where Im signifies "imaginary part of."

For a cloud of independently scattering particles the ratio of K to S is therefore

$$\frac{K}{S} = \frac{\sigma_a}{\sigma_s/2} = \frac{9}{4\pi^3 a^3 \nu^3} \cdot \frac{k}{(n^2 - k^2 - 1)^2 + 4k^2} \qquad (43)$$

where the backscattering cross-section is taken as approximately $\sigma_s/2$.

The reflectance of the cloud is given, as usual, by Eq (16):

$$R_v = 1 + \frac{K}{S} - \sqrt{\frac{K^2}{S^2} + 2\frac{K}{S}}$$

Figure 23 shows the reflectance of the cloud in the region of the scallop for particle diameters of 5μ and 2μ. It is seen that the main features of the scallop are at least qualitatively reproduced.

This agreement with experiment does not necessarily mean that independent dipole scattering is the correct explanation of the scallop since the dipole approximation should not be valid for opaque particles and especially not for particles as large as 122μ for which, as we have seen, the scallop is still found. It is conceivable that the apparent success of the dipole approximation is that the scattering is in fact caused simply by the surface asperities which can be seen in Figure 17.

Further experiments to discriminate between dipole scattering, surface perturbation, and altered optical constants should be carried out.

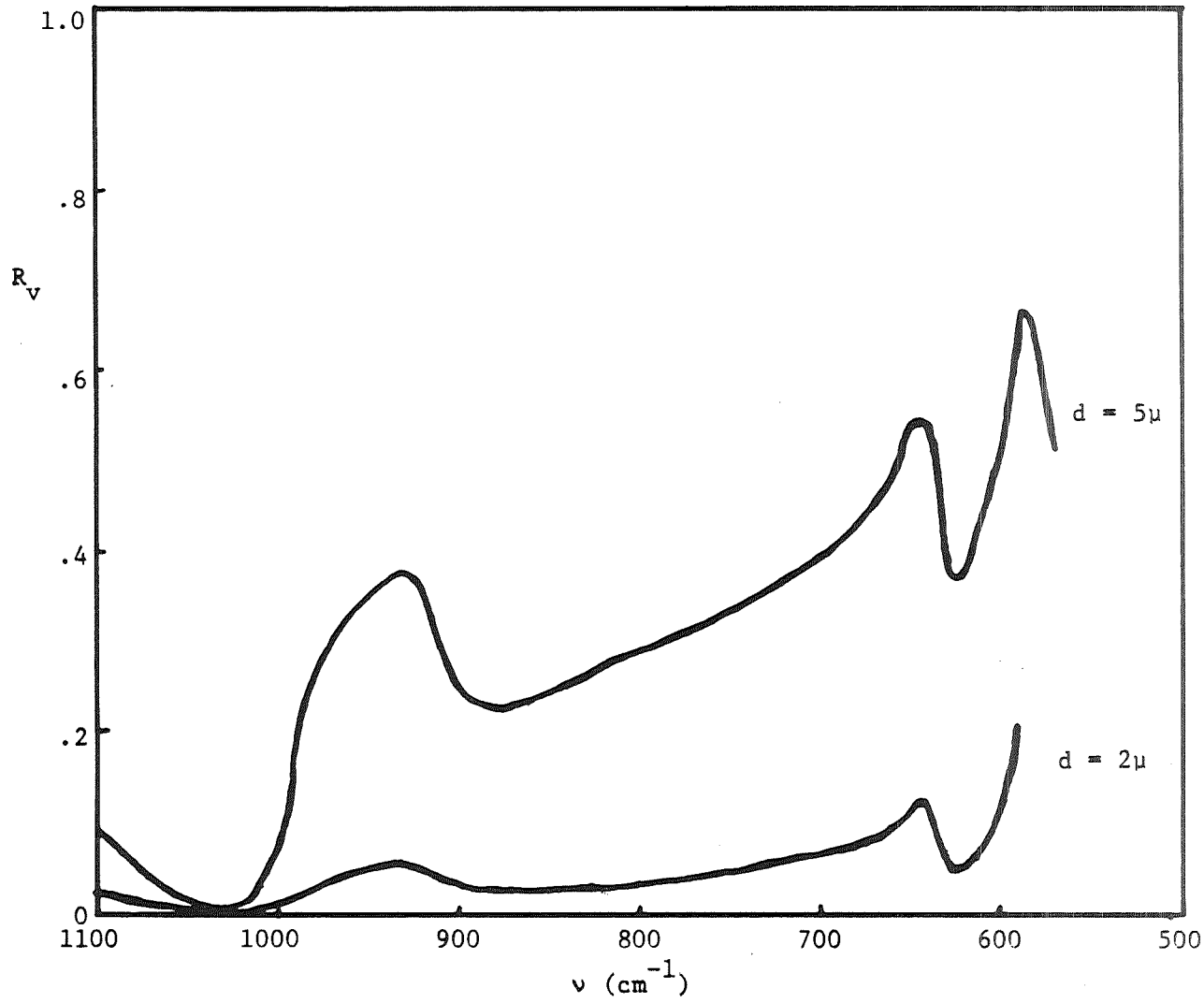

FIGURE 23. THEORETICAL REFLECTANCE OF CORUNDUM ACCORDING TO INDEPENDENT DIPOLE SCATTERING MODEL.

At the present time we believe that the last two hypotheses appear to show considerable promise in having the potential to explain what has been the most puzzling phenomenon encountered in our work. If either of them proves successful, it may very well aid in solving the particle-size dependence problem at the same time.

C. GARNET AND GLASS

During the course of our work we have relied a great deal on the spectra of quartz and corundum. Periodically, questions have arisen as to whether these crystals, which are both hexagonal, might be causing some of our difficulties due to anistropy. While we have not felt this to be a serious problem, we concluded that some experiments on isotropic materials would prove useful. Unfortunately, isotropic minerals with interesting optical properties in the spectral range of interest are rare and when well classified particle sizes for pure materials having well-known optical constants are also required, the list becomes very small. Garnet and glass were chosen and their optical constants derived.

1. Preparation of Samples to be Used in Obtaining Optical Constants

We obtained some 3M spherically shaped "Superbrite" glass beads in the particle size range 20μ to 40μ (29μ average). They have a plate or window glass composition which is 70% SiO_2, 14% Na_2O, ca 12% CaO with traces of Mg and Al according to Mr. Warren Beck of the 3M Company. Unfortunately, we had no infrared optical constant data for these samples. In order to obtain the optical constants to be used for this material, a polished sample of the bulk material was required. An ingot was produced by heating the beads in an iridium crucible. The problem with casting a bulk sample in this manner is to minimize sodium losses. It was found that the minimum time-temperature relationship necessary for producing an easily pourable melt was 1450°C for 2 hours. Discs of 1.5" diameter and 0.5" thickness were cast in polished graphite

dies. Prior to casting, these dies were heated to 475°C, the maximum temperature to which they could be exposed without oxidation of the graphite. To insure against bubble entrapment, the glass was poured into dies in a thin stream. The glass discs were annealed in the graphite dies at 475°C for 15 hours, and then allowed to cool slowly to room temperature in the furnace. Several millimeters were ground from a disc to remove the surface layer and the sample was then polished so as to be suitable for reflectance measurements on our Perkin-Elmer 521 Spectrometer.

As indicated above, our principal concern relating to compositional variations between this glass disc and the original powder has to do with sodium loss from the melt. We therefore decided to check the sodium-to-calcium ratio in the disc and powder using X-ray fluorescence. Our results indicate a relative loss of 12.5% sodium from the disc. Based on the above rough estimate of the composition of the glass provided by the manufacturer of the beads, the Na_2O content dropped from 14% to 12.2% in preparing the disc. The depth of glass to which the X-ray analysis applies is a few microns (0.99 of the Na intensity is derived from a depth of 2.7 microns).

We also obtained three samples of sized garnet powders from the Barton Mines Corporation of North Creek, New York. These samples represent a combination of almandite and pyrope. The chemical analysis is:

SiO_2	41.34%	Al_2O_3	20.36%
FeO	9.72%	CaO	2.97%
Fe_2O_3	12.55%	MgO	12.35%
		MnO	.85%

and the specific gravity is given as between 3.9 and 4.1. The particle size distribution in microns according to Barton Mines as measured by micromerograph is:

Sample	10%	50%	90%
WO	31.2	21.4	9.6
W7	11.5	8.0	4.4
W16	7.4	4.4	2.3

Several large pieces of this material were also obtained from Barton Mines and polished samples of these were prepared for infrared reflectance measurements using our Perkin-Elmer 521 Spectrometer. As the samples are natural materials and do contain some flaws as well as small amounts of some micaceous minerals, we devoted some effort to polishing faces that were relatively pure and flawless. The samples were smaller than is suitable for the Perkin-Elmer reflection attachment so that a black velvet sample holder was used to fill out the unused portion of the incident beam for both the sample and the reference aluminum mirror. The similarity of several runs on different samples (one of which was smaller but appeared visually to be a cleaner sample) was taken to indicate freedom from the micaceous minerals also known to be present in the deposit.

Polarization data for the spectrometer was obtained using a gold wire-grid polarizer. This data is necessary in order to reduce the 30° incidence reflectance measurements to the optical constants.

2. Mathematical Method of Obtaining the Optical Constants

The reflectance data from the macroscopic samples of glass and garnet obtained on the Perkin-Elmer instrument have been used to obtain approximate values of n and k. From a mathematical point of view the basic problem in determining $n(\nu)$ and $k(\nu)$ from given values of $R(\nu)$ is that one must determine two functions from a given single function. As thus baldly stated, the problem is not capable of solution, and one must therefore either obtain a second, independent spectrum[12] or introduce

some kind of an assumption which makes the spectra $n(\nu)$ and $k(\nu)$ not independent of one another.

There are two assumptions that are currently in vogue. The first of these is that $n(\nu)$ and $k(\nu)$ are the real and imaginary parts of a function, $m(\nu)$, which is analytic in ν considered as a complex variable. This assumption has been used to derive the well-known Kramers-Kronig integral formula which, in essence, supplies the needed independent spectrum (namely, the phase spectrum) which, together with the given amplitude spectrum, enables one to find $n(\nu)$ and $k(\nu)$.

The other assumption (not inconsistent with the assumption of analyticity) involves a more specialized physical model of the behavior of the reflecting medium. The assumption is made that the spectrum is due to a number of simple resonances ("Lorentz lines"). According to the classical dispersion theory we may write the complex dielectric constant in the form

$$\varepsilon(\nu) = \varepsilon_\infty + \sum_{j=1}^{N} \frac{4\pi\rho_j}{1 + i\gamma_j\left(\frac{\nu}{\nu_j}\right) - \left(\frac{\nu}{\nu_i}\right)^2} \tag{44}$$

and it is simply necessary to adjust the parameters N, ε_∞, ρ_j, γ_j, and ν_j so that the values of $R(\nu)$ calculated from Eq (44) and the Fresnel equation agree with the measured values of $R(\nu)$. It is customary to resort to the device of "least squares" to find the "best" values of the parameters in order to overcome the effects of noise in the measured reflectance spectrum.

We have employed the second assumption to try to obtain approximate values of the functions $n(\nu)$ and $k(\nu)$, and have combined this with the "least squares" approach. The measured and fitted spectra from the

samples of glass and garnet are shown in Figures 24 and 25, respectively. It will be observed that both of the fitted spectra leave something to be desired.

With reference to the glass spectrum it will be seen that over rather wide bands the measured values fall consistently above or below the fitted curve, even though the "least squares" criterion was met in this case. There is some question as to whether the form of Eq (44) is really a proper one to describe the physical situation.

In the case of the garnet spectrum, the fitted curve is quite good in most regions, although the parameters used are not such as to meet the "least squares" criterion very well. In particular, there is a serious discrepancy between the fitted and measured spectra in the region of the line whose peak is at $\nu = 480\ cm^{-1}$. There seems to be also a consistent error at the high frequency end of the spectrum, where structure is lacking, although this may not be significant.

One conclusion that we may draw is that it is perhaps preferable to appeal only to the principle of analyticity (which includes the special case of simple Lorentz line resonances) and to replace Eq (44) by the more general form

$$\varepsilon(\nu) = \frac{\sum_{j=0}^{M} a_j \nu^j}{1 + \sum_{j=1}^{N} b_j \nu^j} \qquad (45)$$

While Eq (44) is still specialized to some degree, it is true in principle that any analytic function can be approximated arbitrarily well by Eq (45) over a finite range of the variable ν if only M and N be taken sufficiently large. Such a function as represented by Eq (45) has in fact been used to fit measured spectra of lumped-constant electric circuits. Obviously, the poles in (45) must be restricted to lie in one half-plane to satisfy the demands of the Law of Causality.

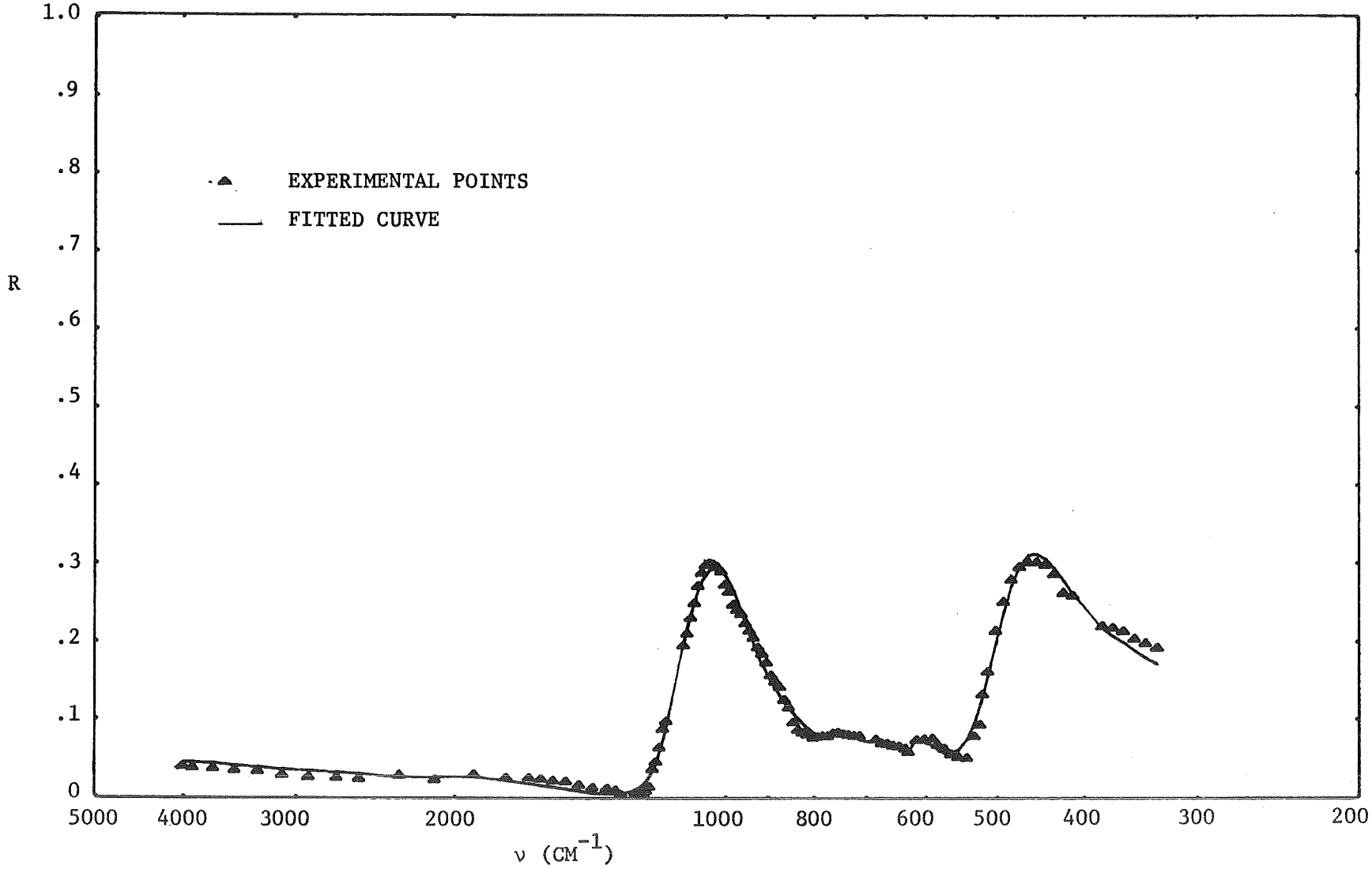

FIGURE 24. REFLECTANCE SPECTRA OF GLASS OBTAINED BY MEASUREMENT AND BY A LEAST SQUARES FIT BASED ON DISPERSION THEORY.

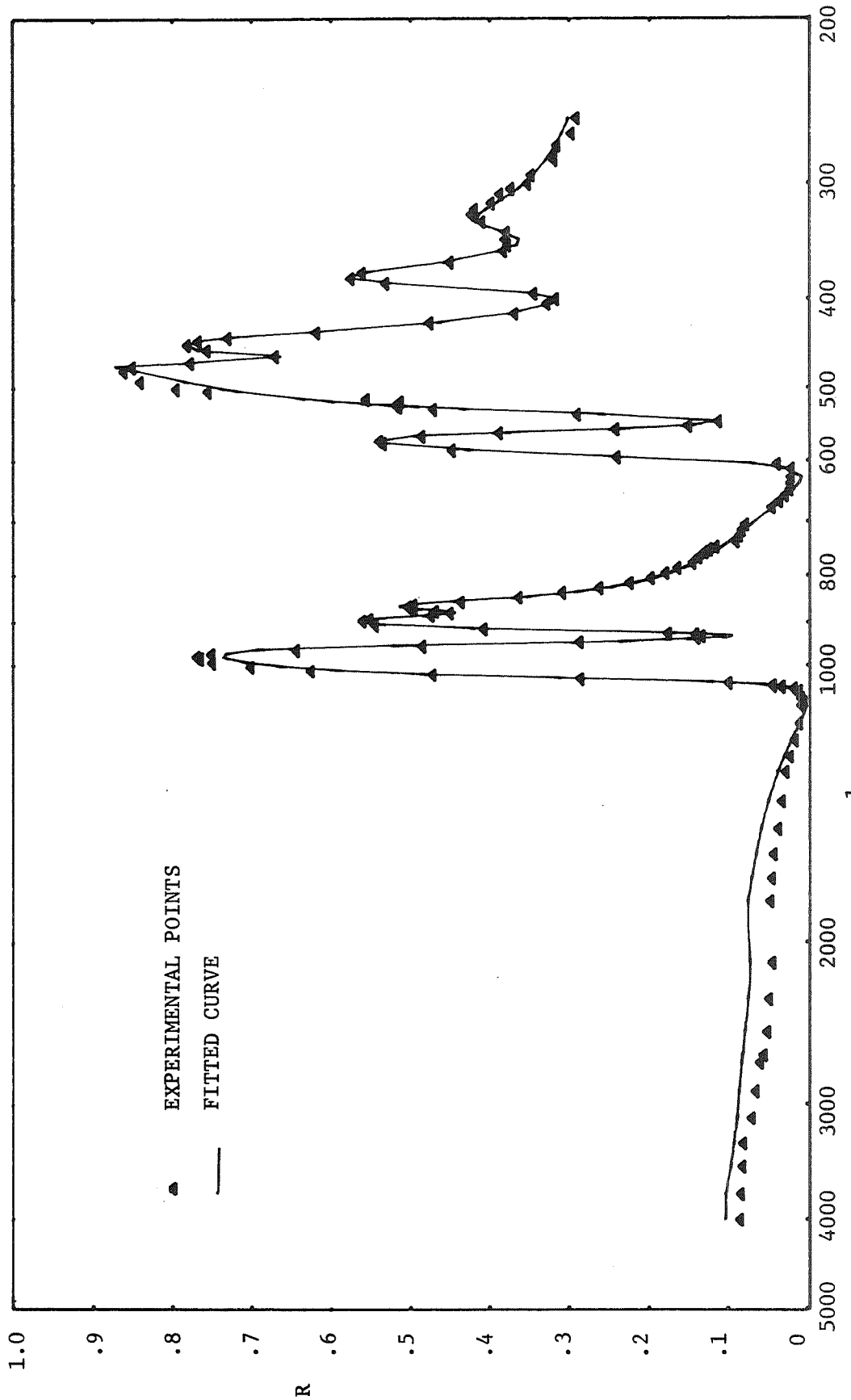

FIGURE 25. REFLECTANCE SPECTRA OF GARNET OBTAINED BY MEASUREMENT AND BY A LEAST SQUARES FIT BASED ON DISPERSION THEORY.

3. Results

Despite the difficulties involved such as sodium loss in preparing the bulk sample of the plate glass, the sampling and geometrical problems in measuring the reflectance of the garnet crystal and the fitting problems in the derivation of the optical constants, we have used these optical constants to make comparison of the theory with experimental data. Figure 26a shows our emittance measurements for the garnet powders. Figure 26b shows several theoretical curves computed by the coarse-particle theory from the derived optical constants. As can be seen, the fit to the WO ($d \sim 21\mu$) powder is quite remarkable. It differs from the experimental data principally in the region of the optical constant fitting problems near 480 cm^{-1} as might be expected. The finer samples experimentally appear to have diminished contrast. The finest garnet powder ($d \sim 4.4\mu$) is not well fitted by theory and we assume that improvements in our fine-particle theory are required. It is interesting to observe that the discrepancies between experiment and coarse-particle theory seem to appear near $d = \lambda$.

The spectrum of Superbrite glass beads was measured and is shown in Figure 27, together with reflectance data obtained (under lower resolution) by the National Bureau of Standards. Also shown is the theoretical fit to these data. Our experimental results appear to show some discrepancies near 1100 cm^{-1} and 450 cm^{-1}. These may be due to small deviations from blackbody behavior of our 3M black paint as suggested to us by Dr. A. Lefohn of the Manned Spacecraft Center, NASA. To test this idea, we ran the glass-bead data against the masking tape data used in our monolayer experiment. The results shown in Figure 28 appear to confirm the idea. However, as we do not know the emissivity of the masking tape, this curve while indicative should not be considered final. The cavity, it should be recalled, is also coated with the 3M black paint. Mr. V. Weidner of the National Bureau of Standards informs us that the 3M black paint does have a reflection peak of 11% between 1050 cm^{-1} and 1100 cm^{-1}. This would be considerably reduced in our

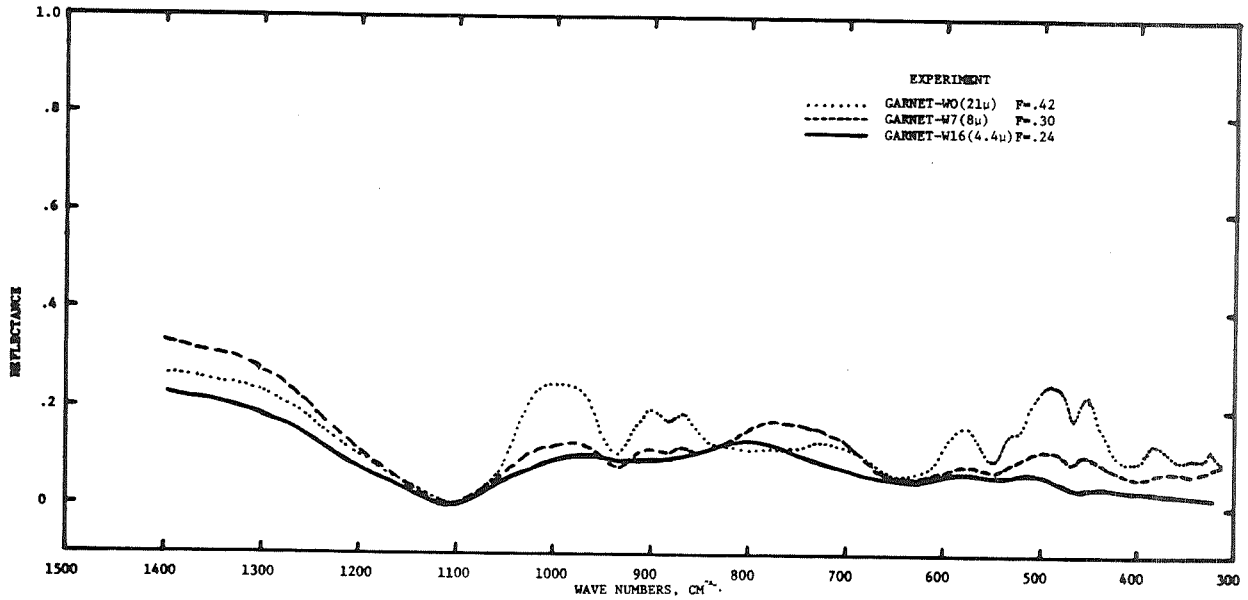

FIGURE 26a. EXPERIMENTAL REFLECTANCE OF GARNET POWDERS.

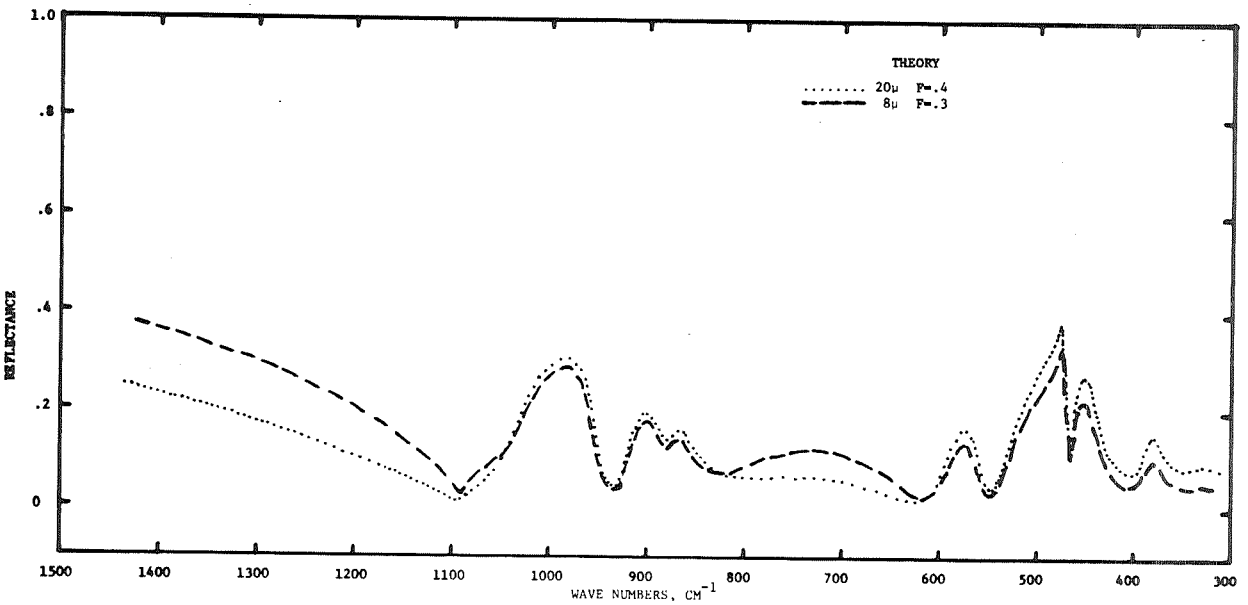

FIGURE 26b. THEORETICAL REFLECTANCE OF GARNET POWDERS.

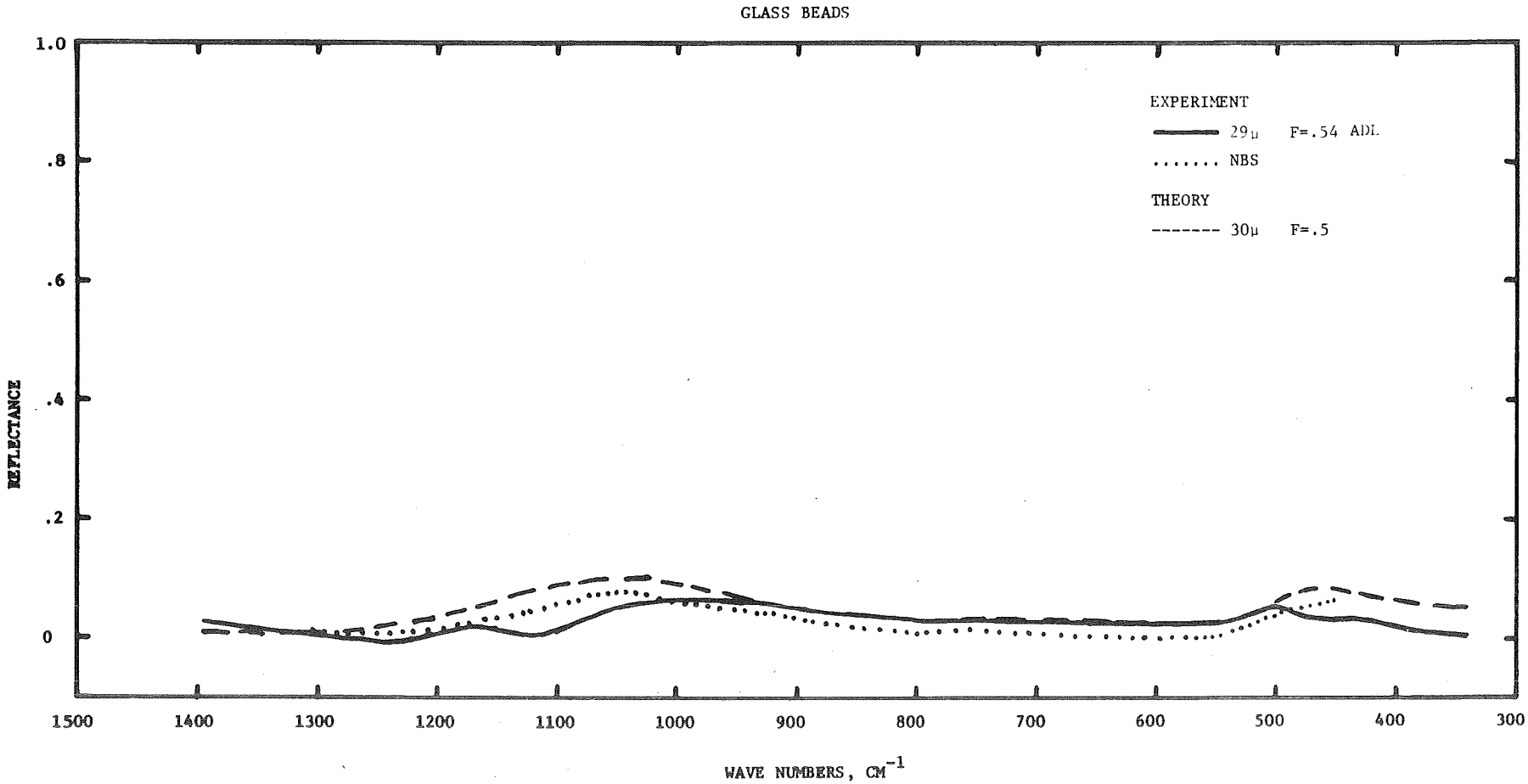

FIGURE 27. COMPARISON OF EXPERIMENTAL AND THEORETICAL REFLECTANCE OF GLASS BEADS.

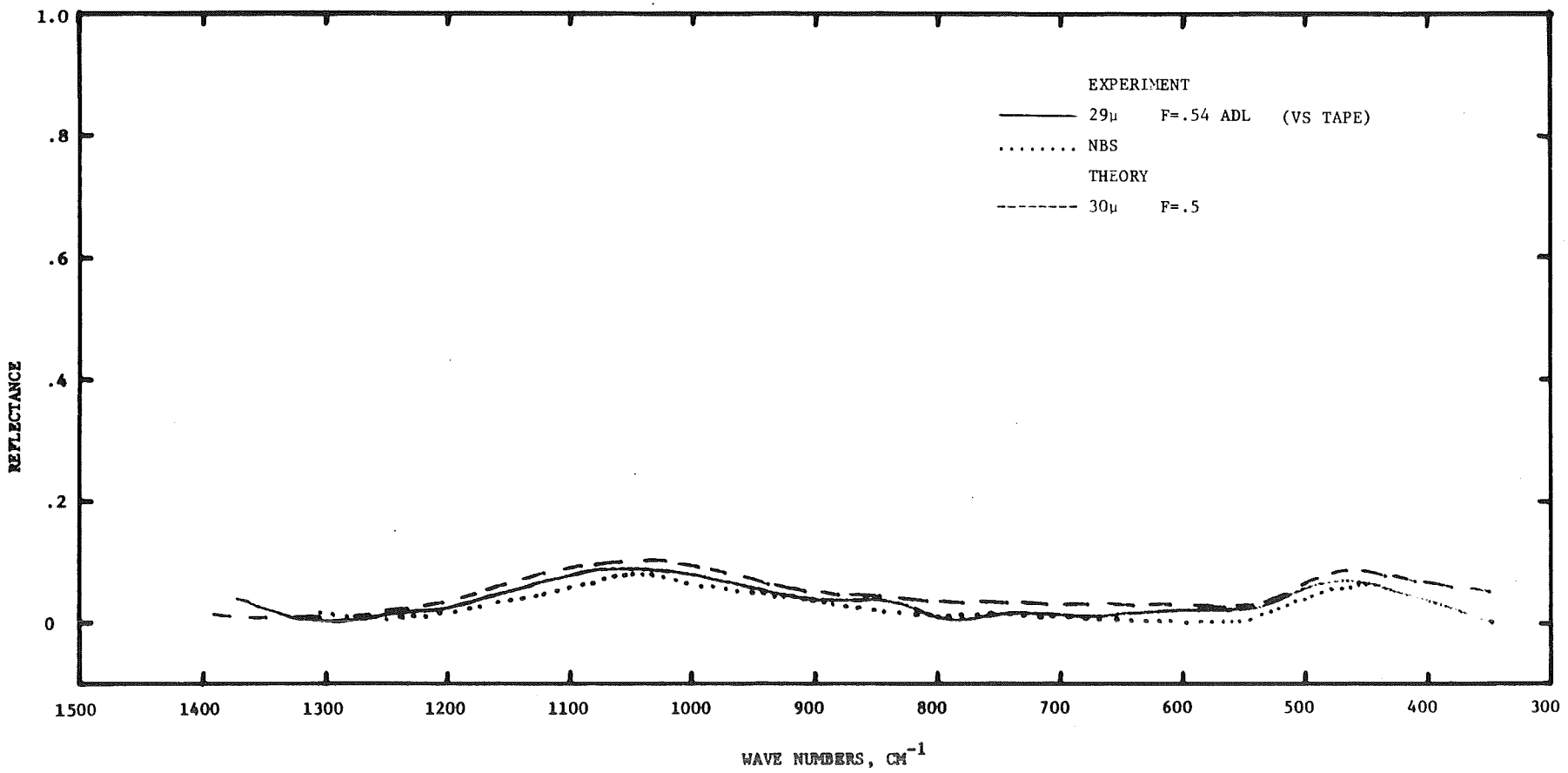

FIGURE 28. COMPARISON OF EXPERIMENTAL AND THEORETICAL REFLECTANCE OF GLASS BEADS (USING TAPE REFERENCE).

experiments due to the 30° grooves of our blackbodies. Nevertheless, it now appears to have caused the spurious results for the glass beads, as well as the hitherto surprising result that our corundum curves appeared to have a higher emittance at 1080 cm^{-1} than at the Christiansen frequency at 1020 cm^{-1}. The discrepancies caused by the deviations from blackbody behavior of our reference blackbodies appear to be most serious in cases of very high sample emittance.

D. MIXTURES OF MINERALS

The excellent fits obtained during the current year's work particularly for the coarse-particle theory suggested that we are now ready to test the mixing rules developed in the past. It should be recalled that our theory has always been structured to provide results for mixtures as we were convinced that this is necessary for natural materials. The mixing rules have been used in the past in order to represent a mixture of the two sets of optical constants that pertain for uniaxial crystals. While, as shown above, this is not a strictly correct method of representing birefringence, it has sufficed to this point and is unlikely to make any major changes in the theoretical results.

Our first experimental mixtures of minerals were two mixtures of quartz and corundum. The experimental spectra are shown in Figure 29a and the theoretical spectra in 29b. The theoretical spectra were computed using the volume fractions and particle sizes taken from the experiment. As can be seen, the agreement between experiment and theory for the 1:1 mixture by volume is remarkable. The other mixture shows more of the quartz spectrum than theoretically predicted and is possibly the result of incomplete mixing.

Figure 30 shows the results of a mixture of quartz and garnet. As the fine-quartz sample used is poorly fitted by the coarse-particle theory, we have not shown the theoretical fit. The fine-particle theory

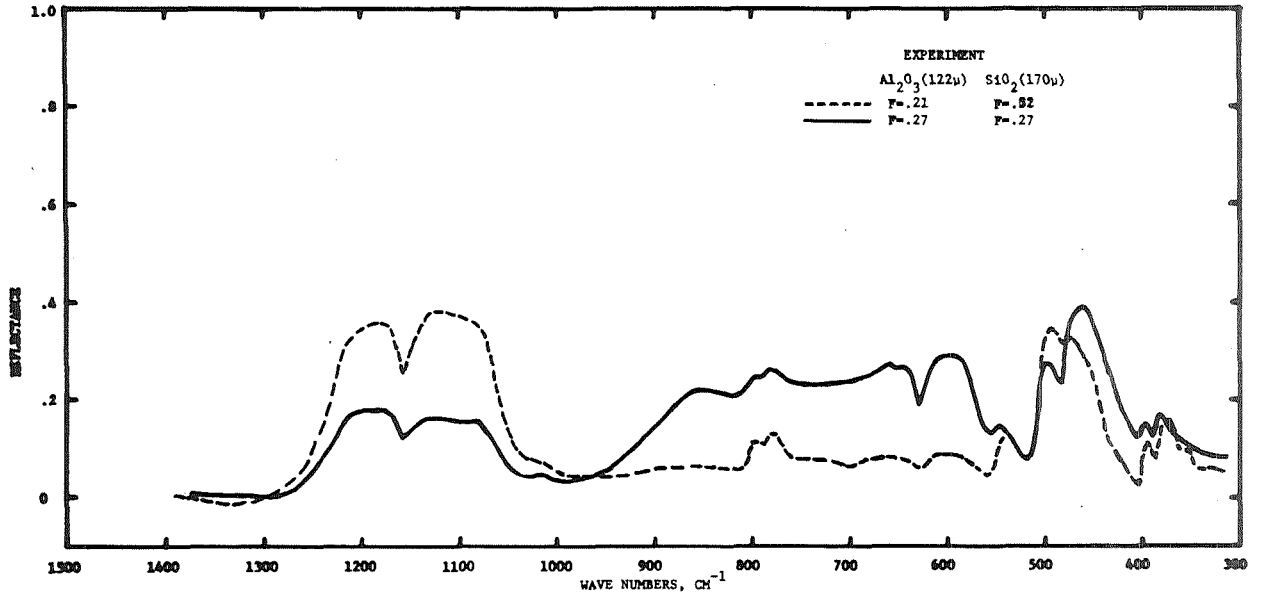

FIGURE 29a. EXPERIMENTAL REFLECTANCE OF MIXTURES OF CORUNDUM AND QUARTZ POWDERS.

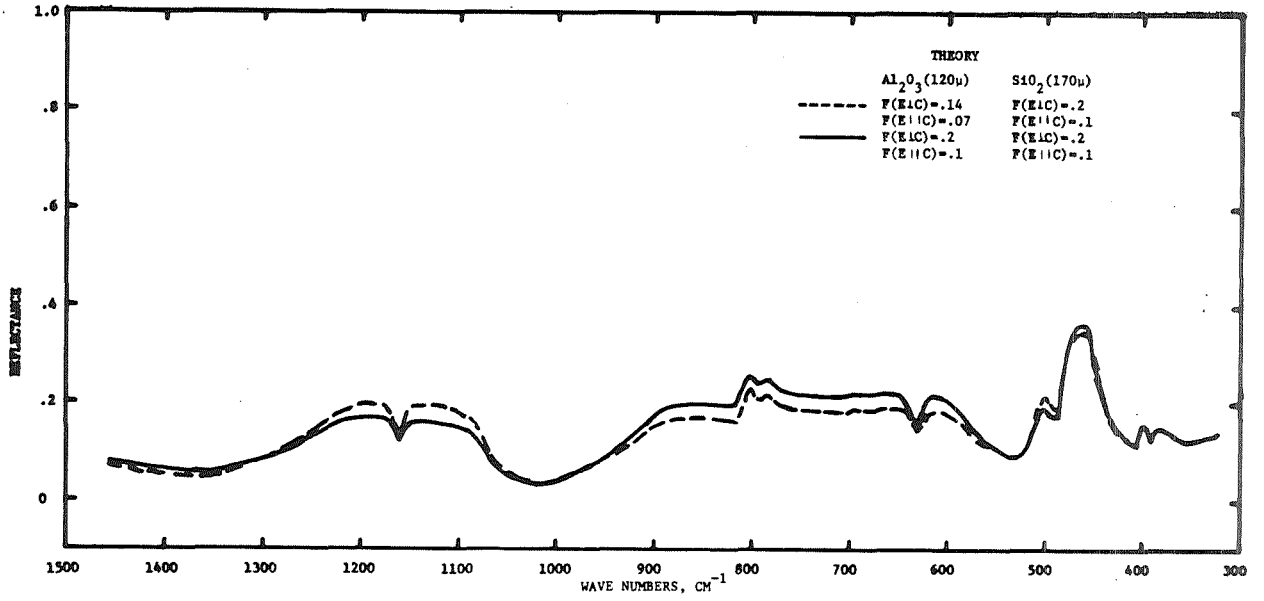

FIGURE 29b. THEORETICAL REFLECTANCE OF MIXTURES OF CORUNDUM AND QUARTZ POWDERS.

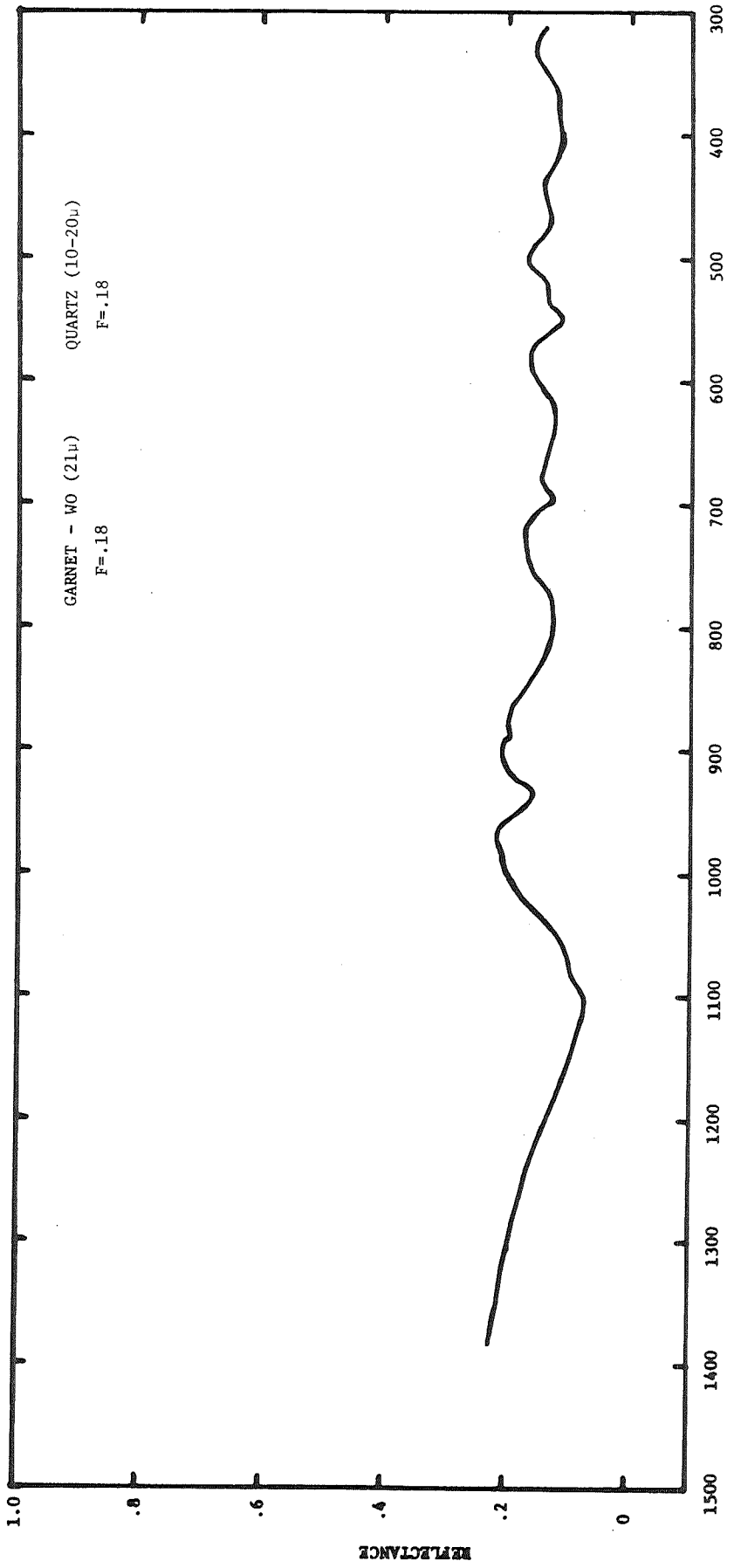

FIGURE 30. EXPERIMENTAL REFLECTANCE OF MIXTURE OF QUARTZ AND GARNET POWDERS.

fits the spectrum of these quartz particles better in some regions so that an adequate fit requires the completion of our work on bridging the two theories.

V. CONCLUSIONS

The current year's work has provided significant improvements in theory of reflectance of particulate materials. These improvements include some simplification of the previous theory by redefinition of the diffuse intensity in the sample, thereby permitting the omission of the surface terms. They also take into account the effects of the finite depth of penetration of radiation into individual particles in both the coarse- and fine-particle theories. Furthermore, a contact factor based on wave interference effects in the gaps between particles has been derived. This factor provides a better transition between the coarse- and fine-particle regimes in that it gradually allows wave optic effects to moderate the strictly geometrical optic approach of the coarse-particle theory. These changes have resulted in a theoretical model that for the first time predicts, at least qualitatively, the correct trend of all reflection features with particle size. At the present time the theory is unable to correctly produce the shape of the reflectance spectrum in the region of anomalous dispersion where $n << 1$. However, surprisingly, a fit to the experimental spectrum can be obtained with a simple dipole scattering mode. This model needs further investigation.

The experimental results on a variety of samples have led us to conclude that the present coarse-particle theory is applicable down to $d \sim \lambda$. While the current fine-particle theory produces some of the features observed in the experimental data, it clearly needs further modification particularly in order to account properly for the reflectance level.

High resolution measurements on different sizes of quartz and corundum powders (the latter having both platelet and chunky shapes) have been carried out. The particle shape does not appear to have a substantial effect on the spectrum. The largest corundum particles (122μ) show the presence of the scallop feature preciously observed only with finer particles. We have also run samples of glass spheres and

garnet powders in order to test the applicability of the theory to the simpler cases of materials without birefringence. For these samples, we found it necessary to obtain optical constants by fitting observed specular reflectance measurements using classical dispersion theory. The present coarse-particle theory gives a good fit to the glass spheres and the larger particle sizes of garnet.

Finally, we have made experimental measurements on several mixtures of minerals and have shown the coarse-particle theory is capable of predicting the resultant spectrum.

VI. SUGGESTIONS FOR FUTURE WORK

We believe that future work should be directed towards:

1. Understanding the discrepancies between theory and experiment in the spectral regions of $n \ll 1$.

2. Refinement of the theory to give a more quantitative account of the particle-size dependence of the powder spectrum.

3. Refinement of the fine-particle theory to take account of clumping phenomena.

4. Further theoretical work on the precise form of the criterion to be used in merging the coarse- and fine-particle theories.

5. A more complete analysis of the effects of birefringence on the spectrum.

6. Development of a quantitative method of correcting observed data for the effect of temperature gradients.

7. Application of the theory of reflectance to the ultimate problem of analysis of the spectrum of an unknown mixture.

VII. APPENDIX

A. DATA REDUCTION PROCEDURE

The spectral emittance $\varepsilon_s(\nu)$ of the sample is the spectral radiance $N_s(\nu)$ of the sample divided by the spectral radiance $B_s(\nu)$ of a blackbody at the same temperature as the sample. We calculate $B_s(\nu)$ from the Planck function using the inferred surface temperature of the sample. We determine $N_s(\nu)$ from the measured output spectrum $E_s(\nu)$ of the sample by means of the instrument transfer function and a correction for radiation, from the environment, that is reflected from the sample.

The transfer function relates radiance $N(\nu)$ to spectral output voltage $E(\nu)$ obtained by Fourier transformation of the interferogram. We assume that the formula is linear and of the form

$$N = N_o + \frac{E}{R} \tag{A1}$$

where N_o, the input radiance that produces zero output signal, is equal to the radiance of the instrument in the direction towards the sample. To determine N_o and R we replace the sample successively by two blackbodies at temperatures T_1 and T_2. Then, from (A1)

$$\varepsilon_1 B_1 = N_o + \frac{E_1}{R} \tag{A2}$$

$$\varepsilon_2 B_2 = N_o + \frac{E_2}{R} \tag{A3}$$

where ε_1, ε_2 are the emittances of the "blackbodies," which allow for small departures from perfect blackbody behavior.

From (A2) and (A3) we obtain for $R(\nu)$ and $N_o(\nu)$:

$$R(\nu) = \frac{E_1 - E_2}{\varepsilon_1 B_1 - \varepsilon_2 B_2} \tag{A4}$$

and

$$N_o(\nu) = \frac{1}{2}\left[\varepsilon_1 B_1 + \varepsilon_2 B_2 - \frac{1}{R}(E_1 + E_2)\right] \tag{A5}$$

where E_1, E_2, ε_1, ε_2, B_1, B_2 are functions of ν.

With the sample in place we can now determine the net radiance N_s of the sample from the measured spectral output E_s by means of Eq (A1):

$$N_s = N_o + \frac{E_s}{R} \tag{A6}$$

where R and N_o are known from (A4) and (A5).

On combining (A4) - (A6) we can express N_s directly in terms of the measured quantities E_1, E_2, and E_s:

$$N_s = \frac{1}{2}(\varepsilon_1 B_1 + \varepsilon_2 B_2) + \frac{1}{2}(\varepsilon_1 B_1 - \varepsilon_2 B_2)\left(\frac{2E_s - E_1 - E_2}{E_1 - E_2}\right) \tag{A7}$$

Finally, the emittance ε_s of the sample is computed from the formula

$$\varepsilon_s = \frac{N_s - B_b(1 - \frac{\Omega}{\pi}) - B_o \frac{\Omega}{\pi}}{B_s - B_b(1 - \frac{\Omega}{\pi}) - B_o \frac{\Omega}{\pi}} \tag{A8}$$

which was derived in our previous reports.[1,2] Here B_b is the radiance of the cavity (assumed to be a blackbody) at temperature T_b surrounding the sample, B_o is the radiance of the interferometer aperture (also assumed to be a blackbody at temperature T_o), B_s is the Planck function

for the temperature T_s of the sample, and Ω is the solid angle subtended at the sample by the interferometer aperture. The cavity walls are coated with 3M black paint which together with multiple reflections should make it an almost perfect blackbody.

In the data reduction up to the present we have assumed that the blackbodies are indeed black, so that $\varepsilon_1 = \varepsilon_2 = 1$. We now believe that this is not strictly true at all wavelengths so that the proper values of ε_1 and ε_2 should be measured and inserted in (A4) and (A5).

It is of interest to calculate the error in the determination of ε_s due to an error in the estimation of the surface temperature of the sample. To do this we neglect the small term Ω/π in (A8), so that

$$\varepsilon_s = \frac{N_s - B_b}{B_s - B_b}$$

On differentiating this expression with respect to B_s we obtain

$$\frac{\Delta\varepsilon_s}{\varepsilon_s} = -\frac{\Delta B_s}{B_s - B_b} \approx -\frac{\Delta T_s}{T_s - T_b} \qquad \text{(A9)}$$

where T_s and T_b are the sample and cavity temperatures, respectively. This expression shows that the relative error in ε_s is equal to the error in the estimation of T_s relative to the temperature difference between the sample and the cavity. Since our determination of T_s by means of the embedded thermocouples agrees within about 0.5°C with the temperature obtained by fitting the spectrum to $\varepsilon_s = 1$ at the principal Christiansen frequency and since $T_s - T_b$ is about 15°C under conditions of low temperature gradient in the sample, $\Delta\varepsilon_s/\varepsilon_s$ is of the order of 3%. In the case of low thermal conductivity of the sample, as occurs for an evacuated powder, the sample surface temperature will be limited by the maximum

permissible heater temperature. In such cases T_s is lower, i.e., closer to T_b, and the error in ε_s is larger.

B. EFFECT OF A TEMPERATURE GRADIENT IN THE POWDER

If a temperature gradient is present in the powder, the Kubelka-Munk equations for the ingoing and outgoing radiation intensities I and J must be modified by the addition of a variable volume emission term $KB(\lambda, x)$. The equations then have the form

$$\frac{dI}{dx} + (K + S)I - SJ = KB \qquad \text{(B1)}$$

$$-\frac{dJ}{dx} + (K + S)J - SI = KB \qquad \text{(B2)}$$

where B is the Planck blackbody function and the coordinate x is measured inward from the surface of the powder.

We assume that B varies linearly with x near the surface of the powder over distances of the order of the mean free path of the radiation, i.e.,

$$B = B_s + B_s' z \qquad \text{(B3)}$$

where B_s, B_s' are the blackbody function and its derivative with respect to x corresponding to the temperature T_s at the surface of the powder ($x = 0$).

Under these conditions the solution of the pair of simultaneous equations (B1) and (B2) is

$$I = A\, e^{-\gamma x} + B_s - \frac{B'_s}{K + 2S} \tag{B4}$$

$$J = R_v\, A\, e^{-\gamma x} + B_s + \frac{B'_s}{K + 2S} \tag{B5}$$

where A is an integration constant to be evaluated by the boundary condition at $x = 0$, R_v is the volume reflectance of the powder, and γ is the extinction coefficient. These quantities are given by

$$R_v = 1 + \frac{K}{S} - \sqrt{\frac{K^2}{S^2} + 2\,\frac{K}{S}} \tag{B6}$$

$$\gamma = \sqrt{K^2 + 2KS} \tag{B7}$$

We assume that the powder is surrounded by a blackbody enclosure at temperature T_b for which the Planck function is B_b. Then in the absence of Fresnel reflection at the surface of the powder the boundary condition at $x = 0$ is

$$I(o) + B_b \tag{B8}$$

Therefore, from (B4),

$$A = B_b - B_s + \frac{B'_s}{K + 2S} \tag{B9}$$

The net radiance from the powder is therefore, from (B5),

$$N_s = J(o) = (1 - R_v)B_s + R_v B_b + (1 + R_v)\,\frac{B'_s}{K + 2S}$$

$$= \varepsilon_s B_s + (1 - \varepsilon_s)B_b + (2 - \varepsilon_s)\,\frac{B'_s}{K + 2S} \tag{B10}$$

where ε_s is the true emittance of the powder.

If the temperature gradient is ignored, the radiance is related to an effective emittance ε_s' by the formula

$$N_s = \varepsilon_s' B_s + (1 - \varepsilon_s') B_b \tag{B11}$$

Here we have neglected the very small effect of the aperture of the interferometer. On equating the two expressions for N_s we find for the error in emittance due to the temperature gradient:

$$\Delta\varepsilon_s = \varepsilon_s' - \varepsilon_s = \frac{(2 - \varepsilon_s)}{(B_s - B_b)(K + 2S)} \left(\frac{\partial B}{\partial T}\right)_s \left(\frac{dT}{dx}\right)_s \tag{B12}$$

where we have set B_s' equal to $(\partial B/\partial T)_s (dT/dx)_s$.

Since

$$B_s - B_b \approx (T_s - T_b) \left(\frac{\partial B}{\partial T}\right)_s \tag{B13}$$

we find that

$$\Delta\varepsilon_s = \frac{(2 - \varepsilon_s)}{(T_s - T_b)(K + 2S)} \left(\frac{dT}{dx}\right)_s \tag{B14}$$

VIII. REFERENCES

1. J. R. Aronson and A. G. Emslie, "Development of a Theory of the Spectral Reflectance of Minerals," Report to NASA, Manned Spacecraft Center, October 1969 (Contract NAS 9-8396).

2. J. R. Aronson and A. G. Emslie, "The Influence of Physical Variables on Spectral Signatures of Natural Targets," Report to AFCRL, December 1969 (Contract F 19628-67-C-0343).

3. J. R. Aronson, A. G. Emslie, T. P. Rooney, I. Coleman and G. Horlick, Appl. Opt. 8, 1639 (1969).

4. L. M. Logan and G. R. Hunt, J. Geophys. Res. 75, 6539 (1970).

5. J. E. Conel, J. Geophys. Res. 74. 1614 (1969).

6. W. G. Spitzer and D. A. Kleinman, Phys. Rev. 121, 1324 (1961).

7. "Microabrasives for Industry," Microabrasives Corporation, Westfield, Massachusetts, August 1, 1967.

8. A. S. Barker, Jr., Phys. Rev. 132, 1474 (1963).

9. C. M. Phillippi, "The Absorption and Reflection Character of Infrared Bands of Powdered Inorganic Materials," AFML-TR-68-317.

10. H. G. Häfele, Z. Naturforschung, 18a, 331 (1963).

11. H. C. van de Hulst, Light Scattering by Small Particles (John Wiley and Sons, Inc., New York, 1957).

12. I. Simon, J. Opt. Soc. Am. 41, 336 (1951).

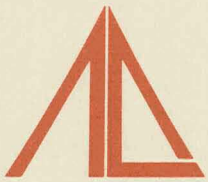

CAMBRIDGE,
MASSACHUSETTS

CHICAGO
NEW YORK
SAN FRANCISCO
WASHINGTON
ATHENS
BRUSSELS
CARACAS
LONDON
MEXICO CITY
PARIS
RIO DE JANEIRO
TORONTO
ZURICH